

Evolution of a novel adrenal cell type that promotes parental care

<https://doi.org/10.1038/s41586-024-07423-y>

Received: 22 March 2023

Accepted: 15 April 2024

Published online: 15 May 2024

 Check for updates

Natalie Niepoth^{1,2,8}, Jennifer R. Merritt^{1,2,8}, Michelle Uminski^{1,2}, Emily Lei^{1,2}, Victoria S. Esquibies^{1,2}, Ina B. Bando^{1,2}, Kimberly Hernandez^{1,2}, Christoph Gebhardt^{1,2}, Sarah A. Wacker³, Stefano Lutz^{4,5}, Asmita Poudel^{6,7}, Kiran K. Soma^{6,7}, Stephanie Rudolph^{4,5} & Andres Bendesky^{1,2,✉}

Cell types with specialized functions fundamentally regulate animal behaviour, and yet the genetic mechanisms that underlie the emergence of novel cell types and their consequences for behaviour are not well understood¹. Here we show that the monogamous oldfield mouse (*Peromyscus polionotus*) has recently evolved a novel cell type in the adrenal gland that expresses the enzyme AKR1C18, which converts progesterone into 20 α -hydroxyprogesterone. We then demonstrate that 20 α -hydroxyprogesterone is more abundant in oldfield mice, where it induces monogamous-typical parental behaviours, than in the closely related promiscuous deer mice (*Peromyscus maniculatus*). Using quantitative trait locus mapping in a cross between these species, we ultimately find interspecific genetic variation that drives expression of the nuclear protein GADD45A and the glycoprotein tenascin N, which contribute to the emergence and function of this cell type in oldfield mice. Our results provide an example by which the recent evolution of a new cell type in a gland outside the brain contributes to the evolution of social behaviour.

Recent advances in molecular profiling have enabled the study of cell types at single-cell resolution both within and across taxa. Using single-cell sequencing, scientists have begun to characterize how assemblages of cell types have arisen over evolutionary time^{2–8} and have identified cell populations that are essential for behaviours including mating, maternal aggression and parental care^{9–11}. However, with some exceptions (for example, in ref. 12), the function of evolutionarily novel cell types has not been firmly established, and the genetics underlying the evolution of new cell types remains largely unknown¹.

Here we leverage the genetic similarity between two sister species of *Peromyscus* mice, the promiscuous prairie deer mouse *P. maniculatus bairdii* (hereafter ‘deer mouse’) and the monogamous oldfield mouse *P. polionotus subgriseus*, to probe the genetic causes and the biochemical and behavioural consequences of a recently evolved cell type in the oldfield mouse adrenal cortex. Owing to their recent evolutionary divergence¹³, these two species can hybridize, enabling forward genetic analysis of traits—including cell-type composition—that have evolved between the two species. As we show here, deer mice and oldfield mice differ markedly in their adrenal gland morphology and function. Using histology and transcriptomics, we characterize the divergence of the adrenal gland at single-cell resolution and identify a novel cell type in oldfield mouse adrenals that synthesizes a hormone derived from progesterone. We then use pharmacology and electrophysiology to evaluate the phenotypic effect of this hormone, and use quantitative genetic mapping methods to identify the genetic loci contributing to the evolution of this cell type.

Large adrenal cortex in oldfield mice

The adrenals are bipartite endocrine glands that secrete catecholamines from the medulla and steroid hormones from the cortex. Catecholamines rapidly modulate physiology, whereas steroid hormones have both fast and slow effects on physiology, neuronal activity and behaviour¹⁴. We observed that the adrenal glands of adult deer mice and oldfield mice differ significantly in size and mass. Whereas the adrenal glands of deer mice and house mice (*Mus musculus*) are similar in size, the adrenals of oldfield mice are fourfold heavier than those of deer mice, and sixfold heavier after adjusting for body weight (Fig. 1a,c). The oldfield mouse adrenal is twofold larger than the deer mouse adrenal at birth, indicating that the size difference has an embryonic origin (Extended Data Fig. 1a). The oldfield mouse adrenal, but not the deer mouse adrenal, then continues to grow throughout adulthood (Extended Data Fig. 1b). This is a highly unusual divergence in internal organ size between closely related species.

Embryologically, the medulla is derived from the neural crest, whereas the cortex is derived from the mesoderm¹⁵. Because the overgrowth could be limited to one of these two tissues, we next measured them individually. We observed that the oldfield mouse cortex is 8.9 times larger by volume than the deer mouse cortex, controlling for body weight, whereas the adrenal medulla is only 2.6 times larger (Fig. 1b,d and Extended Data Fig. 1c). The enlargement of the oldfield mouse cortex is partly due to larger cells (Extended Data Fig. 1d) and partly due to a 4.8-fold increase in the number of cells (Fig. 1e).

¹Zuckerman Mind Brain Behavior Institute, Columbia University, New York, NY, USA. ²Department of Ecology, Evolution and Environmental Biology, Columbia University, New York, NY, USA.

³Department of Chemistry and Biochemistry, Manhattan College, New York, NY, USA. ⁴Department of Neuroscience, Albert Einstein College of Medicine, New York, NY, USA. ⁵Department of Psychiatry and Behavioral Sciences, Albert Einstein College of Medicine, New York, NY, USA. ⁶Department of Psychology, University of British Columbia, Vancouver, British Columbia, Canada.

⁷Djavad Mowafaghian Centre for Brain Health, University of British Columbia, Vancouver, British Columbia, Canada. ⁸These authors contributed equally: Natalie Niepoth, Jennifer R. Merritt.

✉e-mail: a.bendesky@columbia.edu

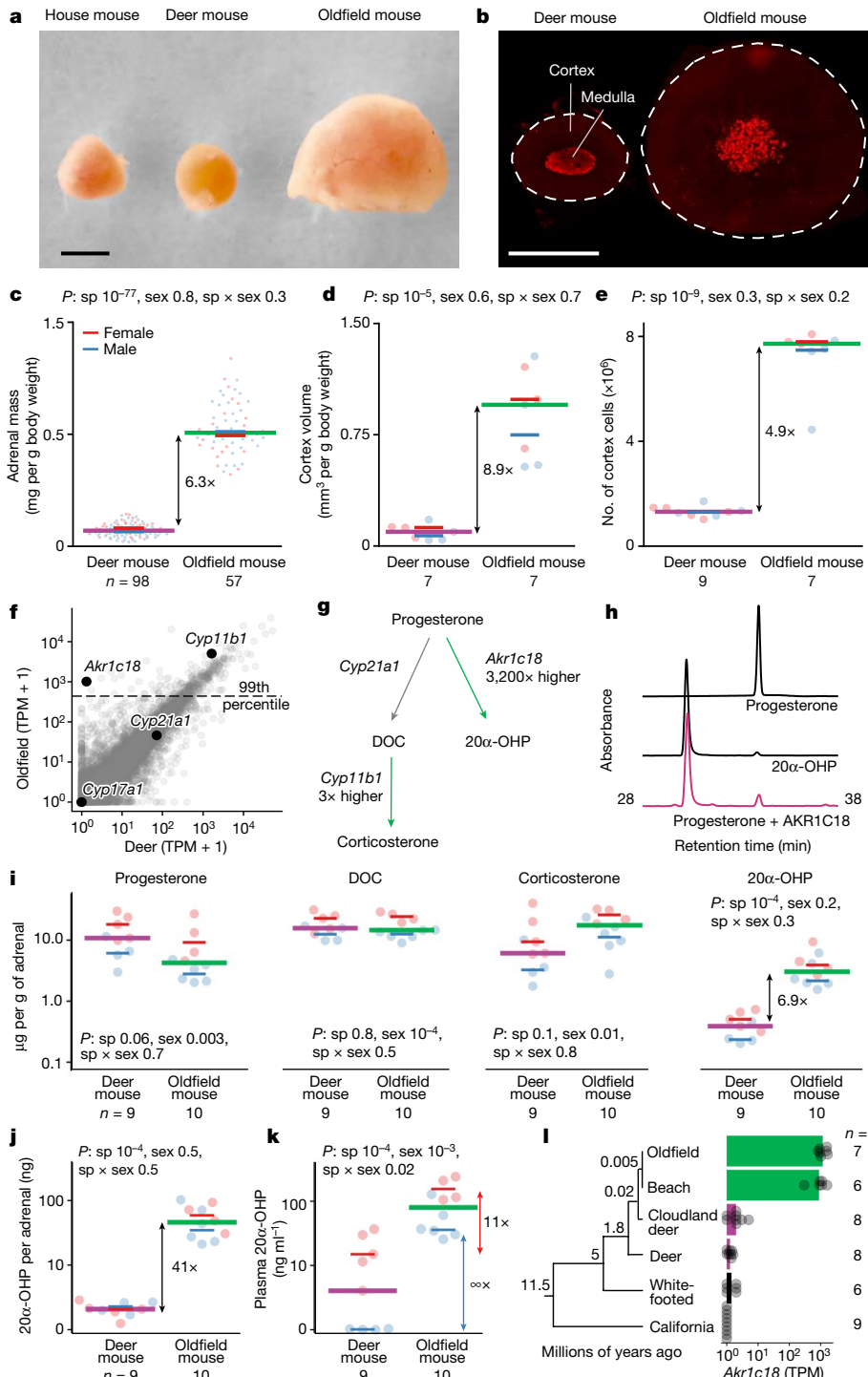


Fig. 1 | Oldfield mice have larger adrenal glands that recently evolved the ability to produce more 20 α -OHP than deer mice. **a**, Adrenal glands from house mouse, deer mouse and oldfield mouse. Scale bar, 1 mm. **b**, Representative mid-adrenal sections from deer mouse and oldfield mouse, labelled with antibody to tyrosine hydroxylase, a marker of the adrenal medulla. The experiment was repeated with 20 individual mice per species with similar results. Scale bar, 1 mm. **c–e**, Species and sex differences in adrenal mass (**c**), cortex volume (**d**) and cortex cell number (**e**). **f**, Scatter plot of adrenal gene expression in deer mice and oldfield mice. TPM, transcripts per million. **g**, Schematic of the enzymatic pathway from progesterone to corticosterone and 20 α -OHP with the fold difference in the expression (oldfield mouse/

deer mouse) of *Cyp11b1* and *Akr1c18*. DOC, deoxycorticosterone. **h**, High-performance liquid chromatography trace of progesterone and 20 α -OHP standards, and the reduction of progesterone to 20 α -OHP by oldfield mouse AKR1C18. **i**, Concentration of steroids in the adrenal, as determined by liquid chromatography tandem mass spectrometry (LC–MS/MS). **j**, Total 20 α -OHP in the adrenal of deer mice and oldfield mice by LC–MS/MS. **k**, Plasma levels of 20 α -OHP, determined by LC–MS/MS. **d,e,i–k**, Key colours as in **c**. **l**, Right, expression of *Akr1c18* in adrenals of *Peromyscus* species, with phylogenetic relationships^{13,20} represented by the dendrogram on the left. **c–e,i–k**, Horizontal lines show medians. *P* values for differences between species (sp), sex, and species and sex (sp × sex) by generalized linear model.

Article

Thus, the oldfield mouse adrenal cortex is much larger than deer mouse adrenal cortex due to a combination of having more cells and larger cells.

Species divergence in adrenal steroids

To begin to characterize the molecular differences between deer mouse and oldfield mouse adrenals, we performed RNA sequencing analysis (RNA-seq) of the whole gland and explored the expression of steroidogenic enzymes. *Cyp17a1*, which is required for the synthesis of cortisol, androgens and oestrogens, was not expressed in the adrenals of either species (Fig. 1f and Extended Data Fig. 1e). Many other rodents, including house mice and voles, also lack adrenal *Cyp17a1* expression^{16,17}. *Cyp21a1*, which converts progesterone into deoxycorticosterone, did not differ in expression between the species (Fig. 1f,g). By contrast, *Cyp11b1*, which converts deoxycorticosterone into corticosterone (the main glucocorticoid in species lacking *Cyp17a1*), was expressed at threefold higher levels in oldfield mice (Fig. 1f,g). The standout difference between species among steroidogenic enzymes was in the expression of 20 α -hydroxysteroid dehydrogenase (encoded by the *Akr1c18* gene), which converts progesterone into 20 α -hydroxyprogesterone (20 α -OHP). *Akr1c18* expression is around 3,200-fold higher in oldfield mice (Fig. 1f,g and Extended Data Fig. 1e,f). *Akr1c18* is expressed at very low levels (mean of <0.5 transcripts per million) in deer mice, whereas it is one of the most highly expressed genes in the gland (>1,000 transcripts per million) in oldfield mice. AKR1C18 does not differ in its amino acid sequence between deer mice and oldfield mice. However, it is only 85–89% identical to house mouse and brown rat AKR1C18 (Supplementary Fig. 1), which have been shown to convert progesterone to 20 α -OHP^{18,19}, raising the possibility that the biochemical activity of AKR1C18 is not conserved in *Peromyscus*. To test this, we incubated progesterone with recombinant deer/oldfield mouse AKR1C18 in vitro and observed that it indeed converts progesterone into 20 α -OHP (Fig. 1h). Together, our molecular results indicate that the expression of 20 α -OHP-synthesizing *Akr1c18* has diverged substantially between oldfield and deer mouse adrenal glands.

Next, we measured the substrates and products of the steroidogenic enzymes encoded by the differentially expressed genes (Fig. 1g,i and Extended Data Fig. 1g). There was no significant difference between the species in the concentration of progesterone, deoxycorticosterone or corticosterone per gram of adrenal. Consistent with the large interspecific difference in expression of *Akr1c18*, its product 20 α -OHP was 6.9-fold more abundant per gram of oldfield mice adrenals. Because oldfield mouse adrenals are much larger, the amount of 20 α -OHP per gland is 41-fold higher than in deer mice (Fig. 1j). Reflecting this large difference in 20 α -OHP in the adrenal glands, the plasma levels of 20 α -OHP are also significantly higher in oldfield mice (Fig. 1k). Deer mouse males have undetectable levels of 20 α -OHP, whereas deer mouse females have more than males, but 11-fold lower concentration than oldfield females. The higher plasma levels of 20 α -OHP in females than males are probably owing to high AKR1C18 expression in the ovaries but not the testes of both species (Extended Data Fig. 1h,i). Consistent with most circulating 20 α -OHP in oldfield mice having an adrenal origin, bilateral adrenalectomy reduced plasma 20 α -OHP to the low levels seen in deer mice (Extended Data Fig. 1j). Thus, divergence in adrenal gene expression between the species, particularly in levels of *Akr1c18*, has had major consequences on steroid hormone levels.

Evolution of adrenal 20 α -OHP production

To pinpoint the evolutionary origin of adrenal 20 α -OHP production in *Peromyscus*, we measured *Akr1c18* expression across two additional *Peromyscus* species—the white-footed mouse *Peromyscus leucopus* and the California mouse *Peromyscus californicus*. We also measured *Akr1c18* expression in a subspecies of *P. polionotus* (the Santa Rosa Island beach mouse *P. polionotus leucocephalus*) and of *P. maniculatus* (the cloudland

deer mouse *P. maniculatus nubiterrae*). *Akr1c18* expression was bimodal, with nearly undetectable levels in all species, except for high levels in the two *P. polionotus* subspecies only (oldfield mice and beach mice) (Fig. 1l). *P. polionotus* diverged from cloudland deer mice (which scarcely expressed *Akr1c18*) within the last approximately 20,000 years²⁰, suggesting a very recent evolution of adrenal *Akr1c18* expression.

20 α -OHP increases parental behaviour

20 α -OHP has long been considered to be an inactive metabolite of progesterone, and little is known about its effects on behaviour²¹. Given the prominent role of steroid hormones in regulating parental behaviours and the higher levels of both 20 α -OHP and parental behaviour in oldfield mice^{13,22}, we hypothesized that 20 α -OHP promotes parental care. To test this hypothesis, we delivered a single systemic dose of 20 α -OHP to oldfield mouse parents and then measured parenting behaviour 20 h later (Fig. 2a). Remarkably, this single dose had a large effect on promoting parental care: it led to more grooming and huddling of pups, retrieving more pups to the nest, and building more robust nests (Fig. 2b). 20 α -OHP also promoted nest building in sexually naive oldfield mice and pup grooming and pup retrieval in deer mice (0% of mice retrieved pups after a control injection whereas 17% did so after 20 α -OHP injection; $P = 0.002$; Extended Data Fig. 2). The effects on parental behaviours were broader and more robust in oldfield mouse parents, suggesting that reproductive status and species shape the response to 20 α -OHP. These results suggest that the evolution of high 20 α -OHP in oldfield mice has likely contributed to their monogamous-typical parental behaviours.

We next tested whether 20 α -OHP affected pair-bonding behaviour, an important component of monogamy, by measuring the preference to huddle with their partner compared with a novel conspecific of the opposite sex²³. Vehicle-injected monogamous oldfield mice huddled with their partner three times as long than with a novel individual; however, this preference was not significantly modified when the mice were injected with 20 α -OHP (Fig. 2c and Extended Data Fig. 3). Promiscuous deer mice did not huddle with either their partner or a stranger, and this behaviour was not altered by 20 α -OHP (Extended Data Fig. 3).

As a test of the effects of 20 α -OHP on a non-social behaviour, we measured anxiety-related behaviour on the elevated plus maze assay, which measures preference for the relative safety of corridors with walls over more exposed corridors without walls. 20 α -OHP did not affect the relative preference for open over closed arms in oldfield mice (Fig. 2d). Together, these findings indicate that 20 α -OHP affects parental behaviours but has no significant effects on pair bonding or on the avoidance of open areas. This suggests that 20 α -OHP modulates neuronal circuits with specificity to parenting and that the acquisition of high 20 α -OHP may have contributed to the evolution of biparental care in monogamous oldfield mice.

20 α -OHP is metabolized into allo-diol

Because 20 α -OHP has weak affinity for the nuclear progesterone receptor^{24,25} and there are no reported effects on other steroid-sensitive receptors, its behavioural effects could be mediated by one of its metabolites. 20 α -OHP can be metabolized into 5 α -pregnane-3 α ,20 α -diol (allo-pregnadiol or, simply, allo-diol) through the actions of 5 α -reductase and 3 α -hydroxysteroid dehydrogenase^{26,27} (Fig. 2e). These enzymes are broadly expressed in brains of rodents and humans^{28–31}, where they also metabolize progesterone into 5 α -pregnane-3 α -ol-20-one (allopregnanolone), a neurosteroid with rapid non-genomic effects on neuronal excitability³². Neurosteroids affect parental behaviour at least partly through receptors in the cerebellum³³. We found that 20 α -OHP was converted to allo-diol in vitro by the cerebellum and the hypothalamus (another key parental care brain region³⁴) of both deer mice and oldfield mice, whereas there was no change in levels of

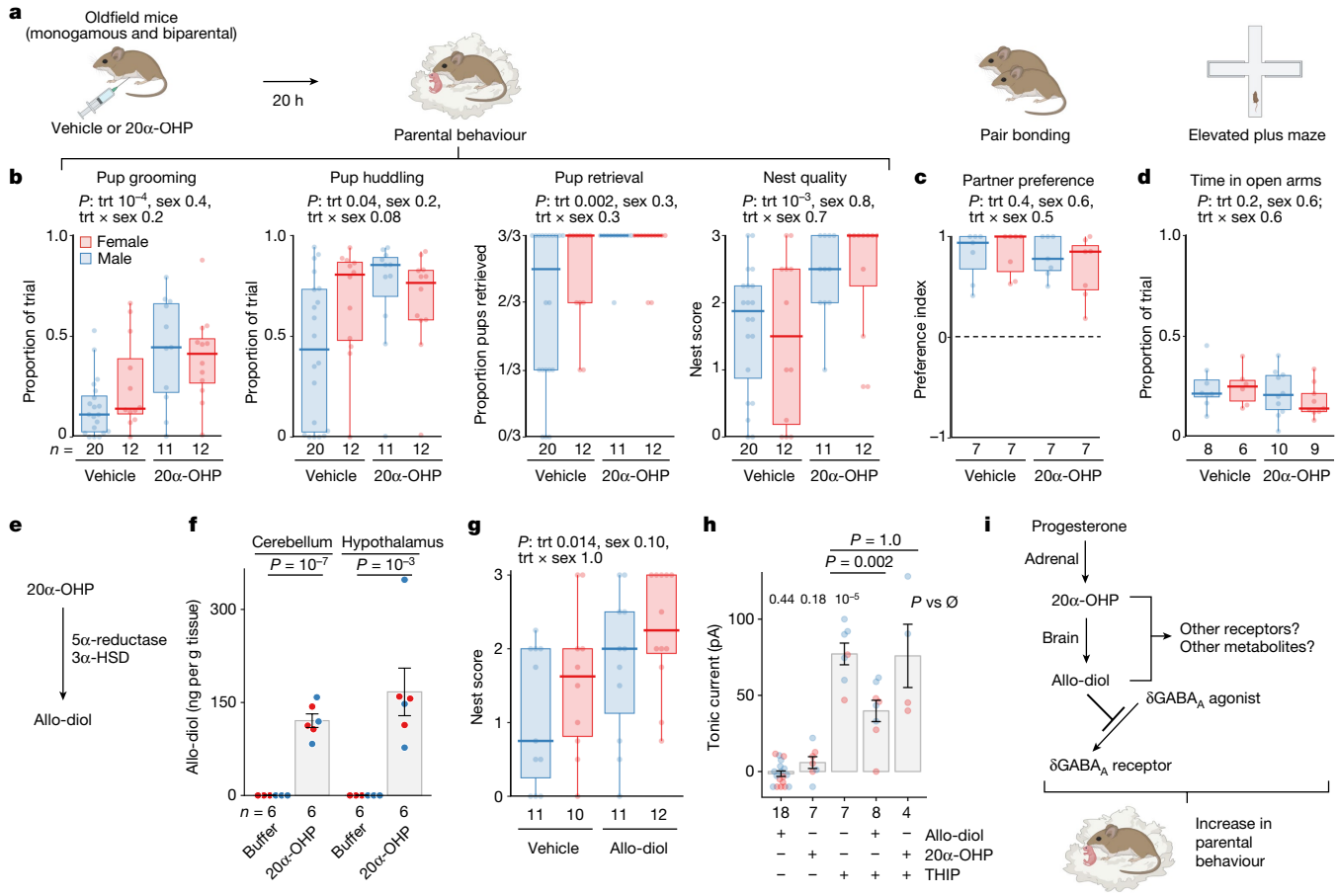


Fig. 2 | 20 α -OHP and its metabolite allo-diol increase parenting behaviours. **a**, Schematic of behavioural assays after administration of 20 α -OHP to oldfield mouse parents. **b**, Parental care as measured by proportion of time spent grooming (licking) and huddling pups, fraction of pups retrieved to the nest and nest quality score (from 0 to 4). **c**, Partner preference as measured by [(time huddling with partner – time huddling with novel conspecific of opposite sex)/(time huddling with partner + time huddling with novel conspecific of opposite sex)]. **d**, Proportion of time spent in the open arms of the elevated plus maze. **e**, Schematic of enzymatic pathway from 20 α -OHP to allo-diol. 3 α -HSD, 3 α -hydroxysteroid dehydrogenase. **f**, Allo-diol concentration after cerebellum and hypothalamus were incubated with 20 α -OHP, for male (blue) and female (red) oldfield mice. Data are mean \pm s.e.m. **g**, Nest quality of oldfield mouse parents after an injection of allo-diol 1 h earlier. **h**, Tonic GABAergic currents recorded from cerebellar granule cells of male (blue) and female (red) oldfield mice after addition of 300 nM allo-diol, 300 nM 20 α -OHP and 500 nM THIP and in the combinations depicted at the bottom. Amplitude is baseline-subtracted. Baseline tonic current was calculated after gabazine application (Extended Data Fig. 5e). Data are mean \pm s.e.m. **b–d,g**, In box plots, the centre line is the median, box edges delineate 25th and 75th centiles and whiskers extend to 1.5 \times interquartile range. **b–d,g**, Pvalues for differences between treatment (trt), sex, and treatment and sex (trt \times sex) by generalized linear model. **i**, Proposed pathways by which 20 α -OHP promotes parental care.

g, Nest quality of oldfield mouse parents after an injection of allo-diol 1 h earlier. **c,d,g**, Key colours as in **b**. **h**, Tonic GABAergic currents recorded from cerebellar granule cells of male (blue) and female (red) oldfield mice after addition of 300 nM allo-diol, 300 nM 20 α -OHP and 500 nM THIP and in the combinations depicted at the bottom. Amplitude is baseline-subtracted. Baseline tonic current was calculated after gabazine application (Extended Data Fig. 5e). Data are mean \pm s.e.m. Pvalues by two-sided two-sample t test and two-sided one-sample t test ($\mu = 0$). **b–d,g**, In box plots, the centre line is the median, box edges delineate 25th and 75th centiles and whiskers extend to 1.5 \times interquartile range. **b–d,g**, Pvalues for differences between treatment (trt), sex, and treatment and sex (trt \times sex) by generalized linear model. **i**, Proposed pathways by which 20 α -OHP promotes parental care.

allo pregnanolone (Fig. 2f and Extended Data Fig. 4). 20 α -OHP incubation also led to a small increase in progesterone, but the absolute levels of allo-diol produced from 20 α -OHP were more than 20 times higher than those of progesterone. This suggests that although small amounts of 20 α -OHP could be back-converted to progesterone, a much larger amount of 20 α -OHP is metabolized into allo-diol (Extended Data Fig. 4).

Notably, a single systemic injection of allo-diol increased pup retrieval 1 h later in sexually naive deer mice from 1% to 12% of mice retrieving pups ($P = 0.005$) (Extended Data Fig. 5a–d). In oldfield parents, a single injection of allo-diol induced nest-building behaviour (Fig. 2g and Extended Data Fig. 5a–d). Thus, high levels of circulating 20 α -OHP in oldfield mice may lead to increased paternal care in part via its conversion to allo-diol, which then acts on neuronal circuits that are important for parenting.

Allo-diol antagonizes δ GABA_A receptors

Allo-diol is a poorly characterized steroid that structurally resembles neurosteroids that reduce neuronal excitability through modulation of

extrasynaptic GABA_A (type A γ -aminobutyric acid) receptors containing the δ subunit^{35–37} (δ GABA_AR). Notably, δ GABA_AR regulate parental behaviour^{33,36,37}, raising the possibility that allo-diol modulates parental care at least partially through δ GABA_AR. Previous research has shown that allo-diol is a positive allosteric modulator of GABA_AR^{38,39}. However, these measurements were made in preparations that do not contain the δ subunit^{32,38,39}. Therefore, we revisited this question by performing whole-cell patch clamp experiments in oldfield mice cerebellar granule neurons, which express high levels of δ GABA_AR and display large tonic currents with high sensitivity to neurosteroids^{35,40} (Fig. 2h and Extended Data Fig. 5e,f). We found that allo-diol has no effect on baseline tonic currents. However, allo-diol significantly reduced tonic currents evoked by the δ GABA_AR-specific agonist THIP, suggesting that allo-diol may inhibit extrasynaptic tonic GABA currents evoked by other endogenous ligands. Similar push-and-pull effects on GABA_AR have been described for combinations of other neurosteroids^{41,42}. In contrast to allo-diol, 20 α -OHP had no effect on tonic currents on its own nor by modulating the effect of THIP. Thus, despite its structural similarities to better-characterized neurosteroids, allo-diol does not act as a

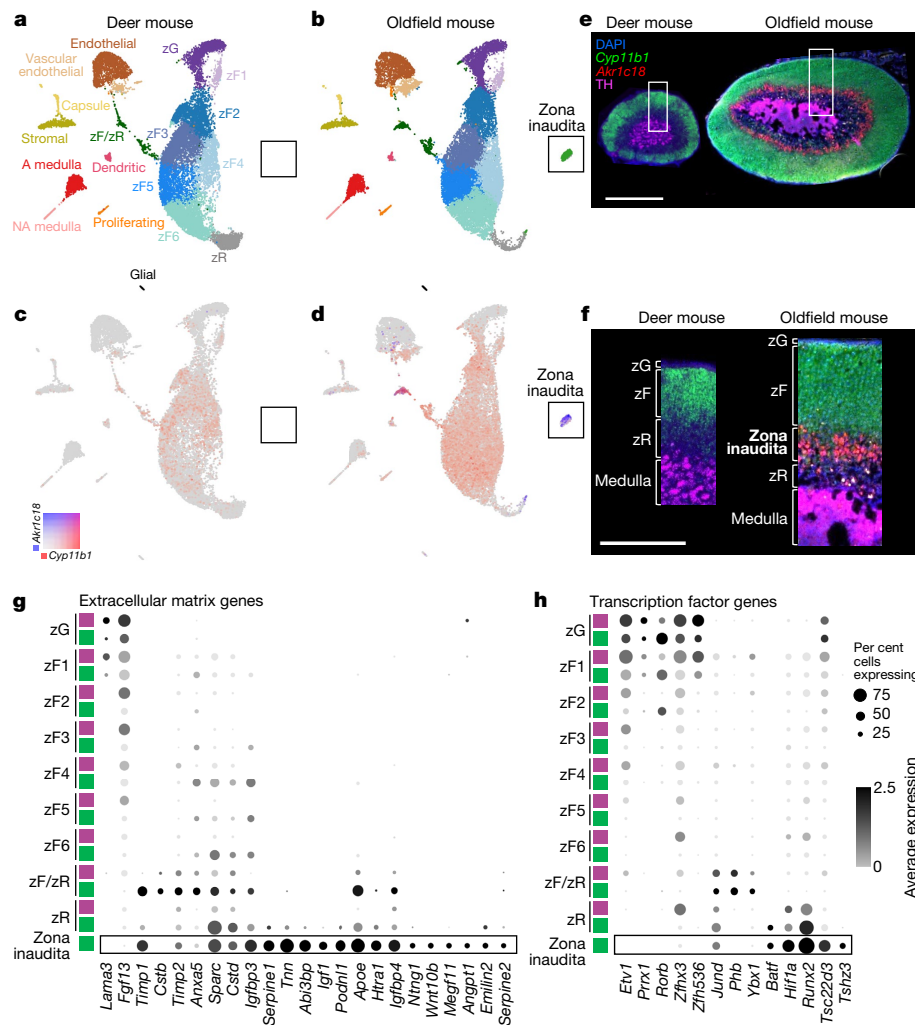


Fig. 3 | Molecular and cellular characterization of adrenal glands reveals the zona inaudita in oldfield mice. **a,b**, Uniform manifold approximation and projection (UMAP) of snRNA-seq data from adrenals of deer mice (**a**) and oldfield mice (**b**). A medulla, adrenergic medulla; NA medulla, noradrenergic medulla; zF, zona fasciculata; zG, zona glomerulosa; zR, zona reticularis. **c,d**, UMAP depicting the expression of *Akr1c18* and *Cyp11b1* in deer mice (**c**) and oldfield mice (**d**). **e**, In situ hybridization of *Cyp11b1* (a marker of zona fasciculata) and

Akr1c18 (marking the zona inaudita) and immunohistochemistry of tyrosine hydroxylase (TH) for visualization of adrenocortical zonation. The zona glomerulosa is characterized by high cell density (Supplementary Fig. 2a). Fifteen biological replicates per species yielded similar results. Scale bar, 1 mm. **f**, Enlarged view of outlined regions in **e**. Scale bar, 0.5 mm. **g,h**, Differential expression of ECM genes (**g**) and transcription factor genes (**h**) across cortical cell types in the adrenals of both species.

typical neurosteroid allosteric modulator, but rather acts as a neutral antagonist of δ GABA_AR. Altogether, our behavioural and electrophysiological results are consistent with a model in which adrenal 20 α -OHP increases parental care at least in part through its conversion in the brain into allo-diol, which modulates δ GABA_AR-mediated inhibition (Fig. 2i).

Oldfield adrenals contain a novel cell type

Our finding that the capacity for 20 α -OHP production in the adrenal is a recently derived trait in *P. polionotus* and that 20 α -OHP influences parental care motivated us to interrogate the evolution of 20 α -OHP production in oldfield mice at the cellular level. We began by conducting single-nucleus RNA-seq (snRNA-seq) of the adrenal glands of both species, as well as of the better-characterized house mouse for comparison. Our analysis identified multiple cell clusters, including endothelial, stromal, glial, medullar and cortical cells, consistent with the known histology of the mammalian adrenal gland (Fig. 3a,b and Extended Data Fig. 6a–c).

The mammalian adrenal cortex is organized into concentric layers with specialized steroidogenic functions¹⁴. An outer zona glomerulosa

produces the mineralocorticoid aldosterone; the middle zona fasciculata produces glucocorticoids such as corticosterone or cortisol; and the innermost zona reticularis produces androgens and oestrogens in some species including humans, but not in many rodents. Based on house mouse, brown rat and human markers for cells in these zones^{43–47}, coupled with histological analyses and the adrenal snRNA-seq data integrated across species, we identified clusters in the snRNA-seq data that define all three layers in both *Peromyscus* species (Fig. 3a–f, Extended Data Figs. 6a–c and 7, Supplementary Note 1 and Supplementary Fig. 2a–c).

Intriguingly, in addition to the three classic steroidogenic cell types, we identified a fourth cellular cluster that also expressed genes that are necessary for steroidogenesis. This cluster was present only in the oldfield mouse adrenal and not in the deer mouse or house mouse (Fig. 3a,b, Extended Data Fig. 6a–c and Supplementary Note 2). Notably, the top-ranked marker of this cell type is *Akr1c18*, which encodes the enzyme that converts progesterone into 20 α -OHP (Fig. 3d, Extended Data Fig. 7 and Supplementary Table 1). In addition to *Akr1c18*, this cell type expresses genes encoding upstream enzymes needed for progesterone production (*Star*, *Cyp11a1* and *3 β -Hsd* (*Hsd3b1* and *Hsd3b6*;

Supplementary Fig. 2d), indicating that these cells can convert cholesterol to 20 α -OHP. By histological staining of *Akr1c18*, we find that this cell type forms a layer between the zona fasciculata and the zona reticularis in oldfield mice and in closely related beach mice (Fig. 3e,f and Supplementary Fig. 2e). As this layer is, to our knowledge, newly described, we called it the zona inaudita.

To characterize how the zona inaudita cell type has diverged from other adrenal cells, we identified genes that are expressed at more than twofold higher levels in zona inaudita cells than in other adrenal cells. We found 194 genes, including *Akr1c18*, that distinguish zona inaudita cells from other adrenal cells (Supplementary Table 1). Although *Akr1c18* is almost completely absent from all deer mouse cells, it is expressed in a subset of non-zona inaudita cells in the oldfield mouse (Fig. 3c,d). Unlike zona inaudita cells, these additional *Akr1c18*⁺ cells co-express *Cyp11b1* yet are located in a scattered manner in the zona reticularis (Fig. 3d,f); we refer to these cells as zF/zR cells. Because adrenocortical cells differentiate as they migrate, it is possible that the zF/zR cells represent a transient state of migrating cells.

The zona inaudita is enriched with marker genes whose protein products localize to the extracellular matrix (ECM) (enrichment $P_{\text{adjusted}} = 10^{-6}$), including core ECM glycoproteins such as tenascin N (encoded by *Tnn*) and *Abi3bp* (Fig. 3g). *Akr1c18* and many ECM zona inaudita markers are among the most differentially expressed genes between the deer mouse and the oldfield mouse adrenals (Extended Data Figs. 6d and 8). Furthermore, the zona inaudita exhibits higher expression of the transcription factor genes *Batf*, *Hif1a*, *Runx2*, *Tsc22d3* and *Tshz3* compared with other cortical cell types; *Tshz3* was not expressed in any cortex cell in deer mice (Fig. 3h and Extended Data Fig. 8).

Together, these results indicate that the zona inaudita cell type is characterized by high levels of *Akr1c18* expression and the upregulation of several transcription factors, as well as by its production of a unique ECM that may contribute to the differentiation and/or maintenance of this adrenal layer.

Evolutionary genetics of zona inaudita

To uncover the evolutionary genetic basis of the emergence of the zona inaudita cell, we used a quantitative genetics approach. We took advantage of the ability of deer mice and oldfield mice to interbreed and characterized the adrenal transcriptomes of a cohort of second-generation (F_2) intercross hybrids (Fig. 4a). Each F_2 individual contains a unique mixture of the genomes of the two species, enabling us to genetically map the interspecific variants that regulate the expression of zona inaudita genes.

We began by measuring the expression of each adrenal gene by bulk RNA-seq of the adrenals of 706 F_2 hybrids (369 males and 337 females). There was substantial sexual dimorphism in the F_2 hybrids, with generally lower levels of *Akr1c18* in females compared to males (Extended Data Fig. 9a). Therefore, to study a more homogeneous group, we focused our analyses on the F_2 males. Next, to characterize the broad genetic architecture of the zona inaudita, we calculated the pairwise correlations between the expression levels of each of the top zona inaudita marker genes among the F_2 hybrids, reasoning that genes whose expression is highly correlated are regulated by an overlapping set of interspecific genetic variants. This analysis revealed two main clusters of correlated genes (Fig. 4b). The first cluster comprised 11 genes, including 2 that encode transcription factors that mark the zona inaudita (*Hif1a* and *Runx2*). We refer to this cluster as the transcription factor module. The second cluster comprised 22 genes, including 12 of the 16 ECM genes that are among the top markers of the zona inaudita, as well as *Akr1c18* (Fig. 4b). We refer to this cluster as the ECM + *Akr1c18* module. The presence of these two groups of correlated genes suggests that genetic variation between the species modulates the expression

of zona inaudita transcription factors and of ECM genes plus *Akr1c18* at least partly independently.

To map the genetic basis of the expression of the zona inaudita transcription factor module, we performed expression quantitative trait locus (eQTL) mapping. Using genome-wide genotypes of F_2 hybrids, we identified the loci at which the genotype (homozygous deer mouse, homozygous oldfield mouse or heterozygous) affects the average expression of the zona inaudita transcription factor module. There were three significant eQTLs, the strongest of which peaked near *Gadd45a*, which encodes a nuclear protein involved in genome stability, cell growth, DNA methylation and differentiation^{48–50} (Fig. 4c). *Gadd45a* is itself a very specific marker of zona inaudita cells (Extended Data Fig. 9b and Supplementary Table 1). The eQTL that maps to *Gadd45a* remains significant after excluding *Gadd45a* expression from the average of the module, showing that genetic variation at that eQTL affects the other genes in the module (Fig. 4c and Extended Data Fig. 9f).

The eQTL mapping to *Gadd45a* suggested that interspecific genetic variation in or near *Gadd45a* modulates the expression of zona inaudita transcription factors in the module. There are no amino acid substitutions between oldfield mice and deer mice at *Gadd45a*. However, eQTL mapping the adrenal expression of *Gadd45a* itself identified a strong eQTL overlapping the *Gadd45a* locus (a *cis*-eQTL) (Fig. 4c): F_2 hybrids that inherited oldfield genetic variants near the *Gadd45a* gene expressed more *Gadd45a* than hybrids that inherited deer mouse variants surrounding *Gadd45a*, suggesting that oldfield mouse-derived *cis*-regulatory variation drives *Gadd45a* expression (Extended Data Fig. 9c). This, in turn, promotes the expression of a cluster of zona inaudita genes including two of its defining transcription factors (Extended Data Fig. 9g).

Notably, neither *Hif1a* nor *Runx2* are located in the three eQTLs for the zona inaudita transcription factor module, nor do they contain *cis*-eQTLs (Fig. 4c and Extended Data Fig. 9d,e). This indicates that genetic variation between oldfield mice and deer mice in these transcription factor markers of the zona inaudita is unlikely to be an important driver of the evolution of this cell type.

eQTL mapping of the zona inaudita ECM + *Akr1c18* module identified four eQTLs (Fig. 4d and Extended Data Fig. 10). Notably, one such eQTL overlapped the *Gadd45a* locus, suggesting that an additional consequence of higher *Gadd45a* expression in oldfield adrenals is also the expression of zona inaudita-specific ECM genes and *Akr1c18*. Conspicuously, *Akr1c18* lacks a *cis*-eQTL, indicating that local genetic variants do not contribute substantially to expression of *Akr1c18* in the oldfield adrenal gland (Fig. 4d and Extended Data Fig. 10j). By contrast, the most prominent *Akr1c18* eQTL is centred on the *Tnn* locus and overlaps an eQTL for the zona inaudita ECM module (Fig. 4d and Extended Data Fig. 10i). *Trans*-eQTLs overlapping *Tnn* were also detected for three of seven individual ECM genes in the module (*Podnl1*, *Serpine1* and *Timp1*), as well as for a non-ECM gene (*Cdkn2a*) in the module (Extended Data Fig. 10d). The results point to this *Tnn*-containing eQTL as a hotspot for modulating the expression of multiple ECM genes specific to the zona inaudita, as well as the functionally relevant gene *Akr1c18*.

Tnn encodes the ECM glycoprotein tenascin N (also known as tenascin W)⁵¹. *Tnn* is one of the most specific markers of the zona inaudita (Extended Data Fig. 9b and Supplementary Table 1) and is essentially undetectable in deer mouse adrenals (Fig. 3g and Extended Data Fig. 10a). The eQTL at the *Tnn* locus that modulates zona inaudita gene expression could be caused by coding or non-coding genetic variation. There were no differences in the TNN amino acid sequence between deer mice and oldfield mice, suggesting that interspecific variation at the eQTL might instead affect the expression of *Tnn* in *cis*. We first tested whether *cis* variation regulates *Tnn* levels by measuring the expression of each of the two alleles in the adrenals of deer mouse × oldfield mouse F_1 hybrids, in which both alleles are present in a common cellular ('*trans*') environment, enabling the measurement of the *cis* effects. Notably, in these F_1 hybrids, nearly all *Tnn* expression

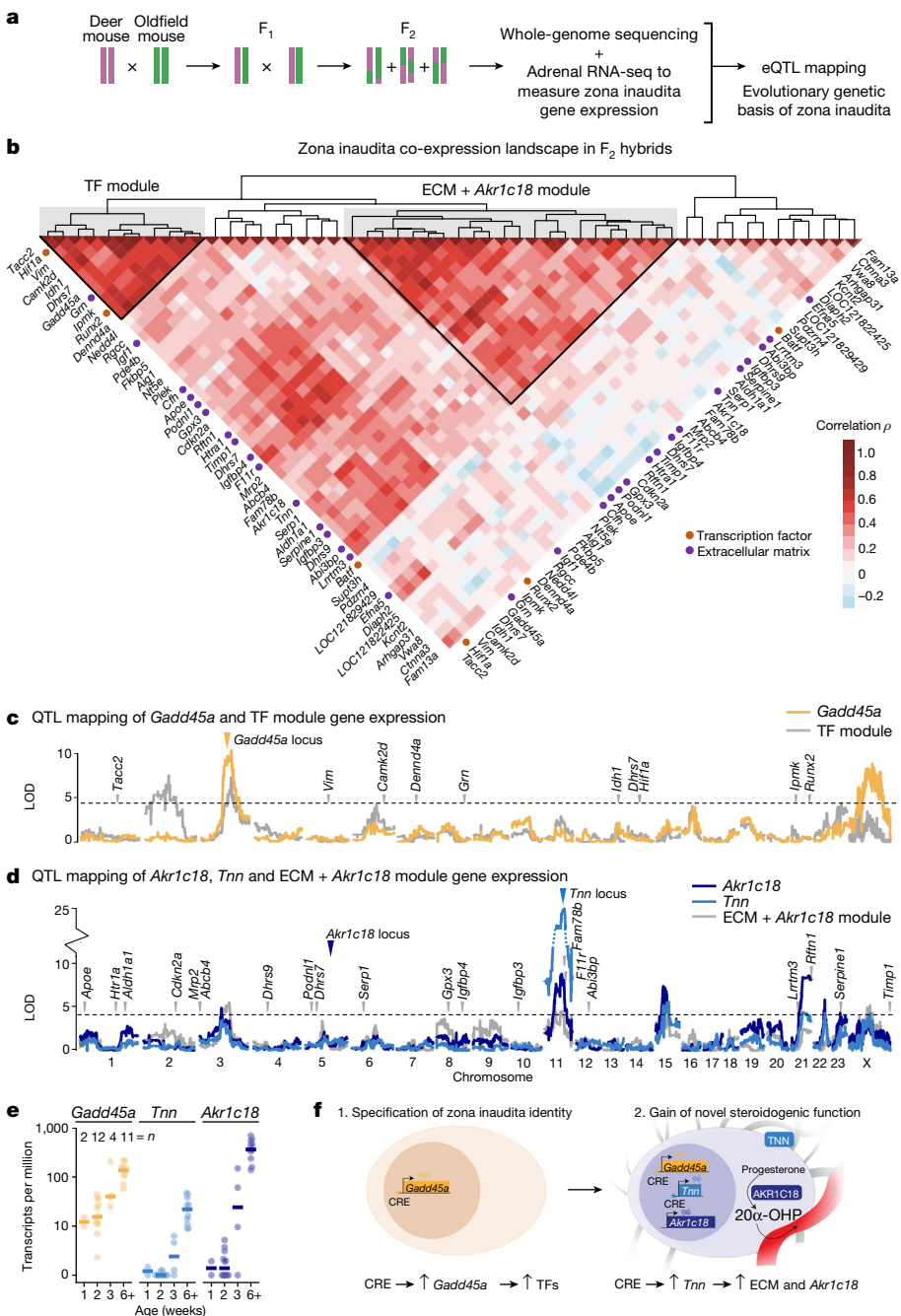


Fig. 4 | Quantitative genetic analysis of zona inaudita identifies prominent roles for *Gadd45a* and *Tnn*. **a**, Schematic of experimental design for eQTL mapping of adrenal zona inaudita genes. **b**, Spearman correlation matrix in F_2 hybrid males of expression of zona inaudita marker genes, defined as four times more highly expressed than in other deer mouse and oldfield mouse adrenal cells. **c**, Logarithm of the odds (LOD) of adrenal expression of *Gadd45a* and the

transcription factor (TF) module across the genome. **d**, LOD of adrenal expression of *Akr1c18*, *Tnn* and the ECM module. Dashed lines denote genome-wide threshold of significance ($\alpha = 0.05$). **e**, Expression of *Gadd45a*, *Tnn* and *Akr1c18* across development in oldfield mice. **f**, Model for acquisition of zona inaudita cell-type identity. CRE, cis-regulatory element. Reproduced with permission from C. Everett.

originated from the oldfield allele (Extended Data Fig. 10b). Consistent with a strong *cis* effect, mapping the expression of *Tnn* revealed a major eQTL encompassing the *Tnn* locus that explained 30% of the variance in expression among the F_2 hybrids (Fig. 4d). The oldfield allele was associated with higher *Tnn* expression, consistent with the effect in the F_1 hybrids (Extended Data Fig. 10h). The expression of *Tnn* and *Akr1c18* is strongly correlated among F_2 mice ($r = 0.70$) and in pure oldfield mice of different ages ($r = 0.97$; Extended Data Fig. 10c), supporting the notion derived from the eQTL mapping that the oldfield allele of *Tnn* promotes *Tnn* expression and this in turn leads to *Akr1c18* expression.

Consistent with a causal relationship between *Tnn* and *Akr1c18*, when we control for *Tnn* expression in the eQTL model of *Akr1c18* expression (a mediation analysis), the eQTL at *Tnn* disappears (Extended Data Fig. 10g). Together, these results suggest that oldfield mouse genetic variants at the *Tnn* locus promote *Tnn* expression and that increased levels of *Tnn* then drive the expression of other zona inaudita genes, including *Akr1c18*.

Three pieces of evidence suggest that genetic variation near *Gadd45a* is important in the development of the zona inaudita cells and that genetic variation at *Tnn* acts later to further shape the differentiation of

these cells. First, the eQTL encompassing *Gadd45a* affects the expression of the ECM + *Akr1c18* cluster, but the eQTL encompassing *Tnn* does not affect the expression of the transcription factor module or of *Gadd45a* itself. This result indicates that genetic variation at *Gadd45a* affects zona inaudita ECM genes but that genetic variation in the ECM gene *Tnn* does not affect *Gadd45a* expression (Fig. 4c,d). Second, *Gadd45a* is appreciably expressed in the adrenal gland by postnatal day 7, whereas robust *Tnn* and *Akr1c18* expression begins after postnatal day 16 (Fig. 4e–f). Third, in a generalized linear model, *Gadd45a* expression explains 41% of the variation ($P = 10^{-84}$) in expression of zona inaudita marker genes among F₂ hybrids, whereas *Tnn* expression explains only 2% of this variation ($P = 10^{-7}$) (Supplementary Fig. 3). We note that whereas genetic variation between oldfield mice and deer mice affecting *Gadd45a* and *Tnn* appears to be particularly important in the evolution of the zona inaudita, additional genetic variation also contributes to the evolutionary emergence of this novel cell type.

Discussion

By combining histology with single-nucleus RNA sequencing, we found the zona inaudita cell, an adrenal cell type without apparent homology to cells in other rodents. By studying the adrenal glands of other species in the genus, we time the emergence of this cell in the monogamous species *P. polionotus* to within the last approximately 20,000 years, a very recent event on an evolutionary timescale.

Using biochemistry and behavioural pharmacology, we then found that the zona inaudita cell is likely to contribute to the high parental care of monogamous oldfield mice by producing 20 α -OHP, a derivative of progesterone. Finally, using transcriptomics and quantitative genetics, we began to characterize the genetic bases of the evolution of this cell type.

Variation in steroid hormone receptors is known to contribute to differences in social behaviours across animals⁵². Here we find a complementary example in which an increase in the levels of 20 α -OHP—a steroid ligand—is likely to contribute to the evolution of more robust parental behaviour in oldfield mice.

Of note, California mice, which evolved monogamy and biparental care independently of oldfield mice, do not express *Akr1c18* in their adrenals, indicating that, even within a genus, social behaviours can evolve convergently through different mechanisms.

20 α -OHP is a poorly studied steroid hormone that is present across mammals, including humans^{53,54}. We found that 20 α -OHP administration increases parental behaviour in oldfield mice, partly through the actions of its metabolite allo-diol, another poorly studied steroid hormone that is also present in humans⁵⁵. Allo-diol, but not 20 α -OHP, negatively modulates tonic GABAergic currents mediated by extrasynaptic δ GABA_ARs, yet it is possible that their behavioural effects in vivo are mediated by additional receptors. Intriguingly, allo-diol acts differently from allopregnanolone, another neurosteroid that positively modulates δ GABA_ARs and is used to treat postpartum depression⁵⁶.

Experimental genetic manipulation in multiple species has shown that transcription factors are essential for the development of particular cell types⁵⁷. Given this essential role in development, genetic variation affecting transcription factors has long been hypothesized to drive the evolution of novel cell types¹, but empirical evidence to support this hypothesis is scant^{58,59}. Here we used unbiased genome-wide genetic mapping rather than a targeted analysis of candidate genes to discover genetic causes of the presence of the zona inaudita cell in one species but not in another. We found that genetic variation affecting *Gadd45a*—a nuclear protein that affects DNA methylation and cell differentiation^{48–50}—probably contributes to the development of the zona inaudita cell, and that genetic variation modulating the expression of tenascin N—an ECM protein—is a likely cause of the gain of a novel enzymatic function of this cell type. Transcription factors are likely to be involved in the development of the zona inaudita cell, as

several transcription factors including *Batf*, *Hif1a*, *Runx2*, *Tsc22d3* and *Tshz3* are also markers of this cell type. However, our genetic mapping experiments indicate that interspecific genetic variation at or near these transcription factor genes is not a major force driving the emergence of the zona inaudita; thus, their expression in the zona inaudita is probably in response to upstream genetic variation in other genes, including *Gadd45a*.

Tnn is one of four members of the tenascin glycoprotein gene family, which are abundantly expressed in the ECM during mammalian embryonic development and are often upregulated in tumours and in adult stem cells⁶⁰. Tenascins regulate cell migration, survival, proliferation and differentiation^{51,61,62} owing to their interactions with many ECM proteins including cell surface receptors and to their capacity for autocrine signalling^{61,63}. *Tnn* is expressed in the zona inaudita cells of oldfield mice but very sparsely in other cells of the oldfield mouse adrenal cortex, and its expression is essentially absent from the adrenals of deer mice, house mice and humans⁶⁴. We found that this novel expression in oldfield mice was largely caused by local non-coding genetic variation. The developmental mechanisms that allow *Tnn* to be expressed specifically in the zona inaudita and by which *Tnn* then promotes the expression of other ECM genes and *Akr1c18*, remain to be further studied.

Altogether, by examining both the genetic causes and the phenotypic consequences of a previously uncharacterized adrenal cell type, our work provides insight into the processes by which novel cell types can arise and their role in the evolution of animal behaviour, even when these cells evolve outside the brain.

Online content

Any methods, additional references, Nature Portfolio reporting summaries, source data, extended data, supplementary information, acknowledgements, peer review information; details of author contributions and competing interests; and statements of data and code availability are available at <https://doi.org/10.1038/s41586-024-07423-y>.

1. Arendt, D. et al. The origin and evolution of cell types. *Nat. Rev. Genet.* **17**, 744–757 (2016).
2. Tosches, M. A. et al. Evolution of pallium, hippocampus, and cortical cell types revealed by single-cell transcriptomics in reptiles. *Science* **360**, 881–888 (2018).
3. Bakken, T. E. et al. Single-cell and single-nucleus RNA-seq uncovers shared and distinct axes of variation in dorsal LGN neurons in mice, non-human primates, and humans. *eLife* **10**, e64875 (2021).
4. Krienen, F. M. et al. Innovations present in the primate interneuron repertoire. *Nature* **586**, 262–269 (2020).
5. Hain, D. et al. Molecular diversity and evolution of neuron types in the amniote brain. *Science* **377**, eabp8202 (2022).
6. Woych, J. et al. Cell-type profiling in salamanders identifies innovations in vertebrate forebrain evolution. *Science* **377**, eabp9186 (2022).
7. Bakken, T. E. et al. Comparative cellular analysis of motor cortex in human, marmoset and mouse. *Nature* **598**, 111–119 (2021).
8. Callaway, E. M. et al. A multimodal cell census and atlas of the mammalian primary motor cortex. *Nature* **598**, 86–102 (2021).
9. Knoedler, J. R. et al. A functional cellular framework for sex and estrous cycle-dependent gene expression and behavior. *Cell* **185**, 654–671.e22 (2022).
10. Kim, D.-W. et al. Multimodal analysis of cell types in a hypothalamic node controlling social behavior. *Cell* **179**, 713–728.e17 (2019).
11. Moffitt, J. R. et al. Molecular, spatial, and functional single-cell profiling of the hypothalamic preoptic region. *Science* **362**, eaau5324 (2018).
12. Brückner, A. et al. Evolutionary assembly of cooperating cell types in an animal chemical defense system. *Cell* **184**, 6138–6156.e28 (2021).
13. Khadraoui, M., Merritt, J. R., Hoekstra, H. E. & Bendesky, A. Post-mating parental behavior trajectories differ across four species of deer mice. *PLoS ONE* **17**, e0276052 (2022).
14. Melmed, S., Koenig, R., Rosen, C., Auchus, R. & Goldfine, A. *Williams Textbook of Endocrinology* 14th edn (Elsevier Health Sciences, 2019).
15. Barresi, M. J. F. & Gilbert, S. F. *Developmental Biology* 13th edn (Oxford Univ. Press, 2023).
16. Keeney, D. S., Jenkins, C. M. & Waterman, M. R. Developmentally regulated expression of adrenal 17 α -hydroxylase cytochrome P450 in the mouse embryo. *Endocrinology* **136**, 4872–4879 (1995).
17. Ogunsua, A. O., de Nicola, A. F., Traikov, H., Birmingham, M. K. & Levine, S. Adrenal steroid biosynthesis by different species of mouselike rodents. *Gen. Comp. Endocrinol.* **16**, 192–199 (1971).
18. Mao, J., Duan, R. W., Zhong, L., Gibori, G. & Azhar, S. Expression, purification and characterization of the rat luteal 20 α -hydroxysteroid dehydrogenase. *Endocrinology* **138**, 182–190 (1997).

19. Velića, P. et al. Lack of functional and expression homology between human and mouse aldo-keto reductase 1C enzymes: implications for modelling human cancers. *Mol. Cancer* **8**, 121 (2009).
20. Wooldridge, T. B. et al. An enhancer of *Agouti* contributes to parallel evolution of cryptically colored beach mice. *Proc. Natl Acad. Sci. USA* **119**, e2202862119 (2022).
21. Kubli-Garfias, C. & Whalen, R. E. Induction of lordosis behavior in female rats by intravenous administration of progestins. *Horm. Behav.* **9**, 380–386 (1977).
22. Bendesky, A. et al. The genetic basis of parental care evolution in monogamous mice. *Nature* **544**, 434–439 (2017).
23. Williams, J. R., Catania, K. C. & Carter, C. S. Development of partner preferences in female prairie voles (*Microtus ochrogaster*): the role of social and sexual experience. *Horm. Behav.* **26**, 339–349 (1992).
24. Ogle, T. F. & Beyer, B. K. Steroid-binding specificity of the progesterone receptor from rat placenta. *J. Steroid Biochem.* **16**, 147–150 (1982).
25. Young, P. C. & Cleary, R. E. Characterization and properties of progesterone-binding components in human endometrium. *J. Clin. Endocrinol. Metab.* **39**, 425–439 (1974).
26. Nowak, F. V., Nuti, K. M. & Karavolas, H. J. Quantitative changes in the metabolism of 20a-hydroxy-4-pregnen-3-one by rat hypothalamus and pituitary during proestrus. *Steroids* **28**, 509–520 (1976).
27. Nowak, F. V. Distribution and metabolism of 20a-hydroxylated progestins in the female rat. *J. Steroid Biochem. Mol. Biol.* **80**, 469–479 (2002).
28. Khanna, M., Qin, K.-N. & Cheng, K.-C. Distribution of 3a-hydroxysteroid dehydrogenase in rat brain and molecular cloning of multiple cDNAs encoding structurally related proteins in humans. *J. Steroid Biochem. Mol. Biol.* **53**, 41–46 (1995).
29. Penning, T. M. et al. Human 3a-hydroxysteroid dehydrogenase isoforms (AKR1C1–AKR1C4) of the aldo-keto reductase superfamily: functional plasticity and tissue distribution reveals roles in the inactivation and formation of male and female sex hormones. *Biochem. J* **351**, 67–77 (2000).
30. Agis-Balboa, R. C. et al. Characterization of brain neurons that express enzymes mediating neurosteroid biosynthesis. *Proc. Natl Acad. Sci. USA* **103**, 14602–14607 (2006).
31. Russell, D. W. & Wilson, J. D. Steroid 5a-reductase: two genes/two enzymes. *Annu. Rev. Biochem.* **63**, 25–61 (1994).
32. Mackenzie, G. & Maguire, J. Neurosteroids and GABAergic signaling in health and disease. *Biomol. Concepts* **4**, 29–42 (2013).
33. Rudolph, S. et al. Cerebellum-specific deletion of the GABA_A receptor δ subunit leads to sex-specific disruption of behavior. *Cell Rep.* **33**, 108338 (2020).
34. Kohl, J. & Dulac, C. Neural control of parental behaviors. *Curr. Opin. Neurobiol.* **49**, 116–122 (2018).
35. Stell, B. M., Brickley, S. G., Tang, C. Y., Farrant, M. & Mody, I. Neuroactive steroids reduce neuronal excitability by selectively enhancing tonic inhibition mediated by δ subunit-containing GABA_A receptors. *Proc. Natl Acad. Sci. USA* **100**, 14439–14444 (2003).
36. Maguire, J. & Mody, I. GABA_AR plasticity during pregnancy: relevance to postpartum depression. *Neuron* **59**, 207–213 (2008).
37. Maguire, J., Ferando, I., Simonsen, C. & Mody, I. Excitability changes related to GABA_A receptor plasticity during pregnancy. *J. Neurosci.* **29**, 9592–9601 (2009).
38. Priestley, C. M., Williamson, E. M., Wafford, K. A. & Sattelle, D. B. Thymol, a constituent of thyme essential oil, is a positive allosteric modulator of human GABA_A receptors and a homo-oligomeric GABA receptor from *Drosophila melanogaster*. *Br. J. Pharmacol.* **140**, 1363–1372 (2003).
39. Belelli, D. & Gee, K. W. 5a-pregnan-3a,20a-diol behaves like a partial agonist in the modulation of GABA-stimulated chloride ion uptake by synaptoneuroosomes. *Eur. J. Pharmacol.* **167**, 173–176 (1989).
40. Farrant, M. & Nusser, Z. Variations on an inhibitory theme: phasic and tonic activation of GABA_A receptors. *Nat. Rev. Neurosci.* **6**, 215–229 (2005).
41. Bixo, M. et al. Treatment of premenstrual dysphoric disorder with the GABA_A receptor modulating steroid antagonist Sepranolone (UC1010)-A randomized controlled trial. *Psychoneuroendocrinology* **80**, 46–55 (2017).
42. Legesse, D. H. et al. Structural insights into opposing actions of neurosteroids on GABA_A receptors. *Nat. Commun.* **14**, 5091 (2023).
43. Dolfi, B. et al. Unravelling the sex-specific diversity and functions of adrenal gland macrophages. *Cell Rep.* **39**, 110949 (2022).
44. Hanemaaijer, E. S. et al. Single-cell atlas of developing murine adrenal gland reveals relation of Schwann cell precursor signature to neuroblastoma phenotype. *Proc. Natl Acad. Sci. USA* **118**, e2022350118 (2021).
45. Huang, L. et al. Single-cell transcriptomes reveal characteristic features of cell types within the human adrenal microenvironment. *J. Cell. Physiol.* **236**, 7308–7321 (2021).
46. Lai, S. et al. Mapping a mammalian adult adrenal gland hierarchy across species by microwell-seq. *Cell Regen.* **9**, 11 (2020).
47. Mitani, F. Functional zonation of the rat adrenal cortex: the development and maintenance. *Proc. Jpn. Acad. Ser. B* **90**, 163–183 (2014).
48. Barreto, G. et al. Gadd45a promotes epigenetic gene activation by repair-mediated DNA demethylation. *Nature* **445**, 671–675 (2007).
49. Wingert, S. et al. DNA-damage response gene GADD45A induces differentiation in hematopoietic stem cells without inhibiting cell cycle or survival. *Stem Cells* **34**, 699–710 (2016).
50. Zhang, R., Shao, J. & Xiang, L. GADD45A protein plays an essential role in active DNA demethylation during terminal osteogenic differentiation of adipose-derived mesenchymal stem cells. *J. Biol. Chem.* **286**, 41083–41094 (2011).
51. Tucker, R. P. & Degen, M. The expression and possible functions of tenascin-W during development and disease. *Front. Cell Dev. Biol.* **7**, 1–10 (2019).
52. Merritt, J. R. et al. A supergene-linked estrogen receptor drives alternative phenotypes in a polymorphic songbird. *Proc. Natl Acad. Sci. USA* **117**, 21673–21680 (2020).
53. Florena, E., Harrison, R., Johnson, M. & Youssefnejadian, E. Plasma 20a-dihydroprogesterone, progesterone and 17-hydroxyprogesterone in normal human pregnancy. *Acta Endocrinol.* **86**, 634–640 (1977).
54. Abdel-Khalik, J., Björklund, E. & Hansens, M. Simultaneous determination of endogenous steroid hormones in human and animal plasma and serum by liquid or gas chromatography coupled to tandem mass spectrometry. *J. Chromatogr. B* **928**, 58–77 (2013).
55. Jensen, C. C. Quantitative determination of urinary pregnanediol and allopregnanediol for clinical use. *Eur. J. Endocrinol.* **18**, 281–287 (1955).
56. Patterson, R., Balan, I., Morrow, A. L. & Meltzer-Brody, S. Novel neurosteroid therapeutics for post-partum depression: perspectives on clinical trials, program development, active research, and future directions. *Neuropsychopharmacology* **49**, 67–72 (2023).
57. Hobert, O. & Kratsios, P. Neuronal identity control by terminal selectors in worms, flies, and chordates. *Curr. Opin. Neurobiol.* **56**, 97–105 (2019).
58. Lynch, V. J. et al. Adaptive changes in the transcription factor HoxA-11 are essential for the evolution of pregnancy in mammals. *Proc. Natl Acad. Sci. USA* **105**, 14928–14933 (2008).
59. Lynch, V. J., May, G. & Wagner, G. P. Regulatory evolution through divergence of a phosphoswitch in the transcription factor CEBPB. *Nature* **480**, 383–386 (2011).
60. Chiquet-Ehrismann, R., Orend, G., Chiquet, M., Tucker, R. P. & Midwood, K. S. Tenascins in stem cell niches. *Matrix Biol.* **37**, 112–123 (2014).
61. Pesheva, P., Gloor, S., Schachner, M. & Probstmeier, R. Tenascin-R is an intrinsic autocrine factor for oligodendrocyte differentiation and promotes cell adhesion by a sulfatide-mediated mechanism. *J. Neurosci.* **17**, 4642–4651 (1997).
62. Kimura, H., Akiyama, H., Nakamura, T. & Crombrugge, B. Tenascin-W inhibits proliferation and differentiation of preosteoblasts during endochondral bone formation. *Biochem. Biophys. Res. Commun.* **356**, 935–941 (2007).
63. Czopka, T., Von Holst, A., Schmidt, G., Ffrench-Constant, C. & Faissner, A. Tenascin C and tenascin R similarly prevent the formation of myelin membranes in a RhoA-dependent manner, but antagonistically regulate the expression of myelin basic protein via a separate pathway. *Glia* **57**, 1790–1801 (2009).
64. Uhlén, M. et al. Tissue-based map of the human proteome. *Science* **347**, 1260419 (2015).

Publisher's note Springer Nature remains neutral with regard to jurisdictional claims in published maps and institutional affiliations.

Springer Nature or its licensor (e.g. a society or other partner) holds exclusive rights to this article under a publishing agreement with the author(s) or other rightsholder(s); author self-archiving of the accepted manuscript version of this article is solely governed by the terms of such publishing agreement and applicable law.

© The Author(s), under exclusive licence to Springer Nature Limited 2024

Methods

No statistical methods were used to predetermine sample size. For behaviour tests, experimenters scoring behaviours were blind to treatment and treatments were randomized. Experimenters were blind to genotype of the F₂ hybrids until analysis.

Animal husbandry

P. maniculatus bairdii (BW stock), *P. polionotus subgriseus* (PO stock), *P. californicus insignis* (IS stock), and *P. leucopus* (LL stock) were originally obtained from the *Peromyscus* Stock Center at the University of South Carolina. *M. musculus* C57BL/6J were obtained from Jackson Laboratories. Mouse colonies were established at Columbia University. Mice were housed under barrier conditions with a 16 h:8 h light:dark cycle at 22 °C and 30–70% humidity. California mice were housed in 30 cm × 23.4 cm × 41.2 cm (916 cm² floor space) ventilated cages (NexGen Rat 900, Allentown), whereas all other species were housed in 19.4 cm × 18.1 cm × 39.8 cm (500 cm² floor space) ventilated cages (NexGen Mouse 500, Allentown). We provided each cage with Enviro-dri (Shepherd Specialty Papers) and cotton nestlets as nest-building material. Mice had access to food (PicoLab Rodent Diet 5053 for nonbreeders, 5058 for breeders) and water ad libitum. All procedures were carried out in accordance with the guidelines established by the NIH Guide for the Care and Use of Laboratory Animals and the Animal Experimentation Guidelines from Columbia University and Albert Einstein College of Medicine. Animal protocols were approved by the Institutional Animal Care and Use Committees of Columbia University and Albert Einstein College of Medicine.

Adrenal mass

Adrenals of deer mice and oldfield mice were dissected, and the periadrenal fat was removed using forceps and fine surgical scissors. To measure adrenal mass, one gland was drop fixed in 4% paraformaldehyde for 30 min and then washed 3 times in PBS. Fixed glands were blotted dry before being weighed on a Mettler Toledo ME103TE Precision Balance.

Adrenal sectioning and marker gene staining

For histology, adrenal glands were dissected, flash frozen in dry ice, and then embedded in cryomolds in optimal cutting temperature (OCT) compound. Glands were sectioned on the horizontal plane using a Leica CM3050S cryostat and mounted on Superfrost microscope slides. Adrenals were sectioned at 10 µm for visualizing cell and nucleus size, and 25–30 µm for visualizing adrenal zonation and the spatial distribution of cell-type markers.

The adrenal medulla was stained using a rabbit anti-tyrosine hydroxylase primary antibody (EMD Millipore AB152, 1:1,000), and the zona glomerulosa was stained using mouse anti-RBFOX1 (EMD Millipore MABE159, 1:1,000). All other genes were stained by *in situ* hybridization using hybridization chain reaction (HCR) v3.0⁶⁵. Split-initiator probes were designed against the deer mouse sequences of aldo-keto reductase family 1 member C18 (*Akr1c18*, annotated as LOC102910062 in the HU_Pman2.1.3 genome), cytochrome P450 11B1 (*Cyp11b1*, annotated as LOC102923554), tenascin N (*Tnn*), and cholesterol side-chain cleavage enzyme (*Cyp11a1*, annotated as LOC102905324) using the HCR 3.0 Probe Maker tool⁶⁶ (up to 33 probe pairs per gene) and ordered as an oligonucleotide pool (oPool) from Integrated DNA Technologies. HCR reagents and hairpin amplifiers were purchased from Molecular Instruments. HCR was performed using the protocol published in ref. 65, and slides were counterstained with DAPI and imaged on a Nikon AZ100 Multizoom microscope or a Nikon Eclipse upright microscope.

Adrenal volume and cell numbers

To measure adrenal cortex and medulla volume, adrenal glands were fixed in 4% paraformaldehyde and then cleared and whole-mount immunostained using the iDISCO+ protocol⁶⁷. The adrenal medulla

marker tyrosine hydroxylase was labelled with rabbit anti-tyrosine hydroxylase primary antibody (Millipore AB152, 1:1,000) and donkey anti-rabbit Alexa Fluor 647 (Invitrogen A-31573, 1:1,000) secondary antibody. Cleared glands were imaged using a LaVision BioTec Ultra-Microscope II light sheet microscope. For each gland, the cortex and medulla were delineated in 20 equidistant z-stack images based on tyrosine hydroxylase expression in ImageJ (v2.1.0), and the cortex and medulla areas were calculated for each image. Volumes of the cortex and medulla, respectively, were estimated by the product of each area × the number of z-stack images per gland × the 3-µm z-stack step size.

The number of cells per gland was estimated by counting the number of DAPI-positive cortical nuclei in a 100 × 100 pixel region of a 10-µm thick cryosectioned adrenal gland. For each individual, cortical nuclei were manually counted in ImageJ (v2.1.0) in six 100 × 100 pixel regions of a single adrenal section (3 regions from the zona fasciculata, 3 from the zona reticularis) and the median nuclei count was calculated. Individual cell area was estimated from the number of DAPI-positive cells per square area, and cell volume was calculated using the equation for volume of a sphere. Bootstrapping was then used to estimate the total number of cortical cells per gland: for each species, cortex volume measurements were sampled with replacement from the original dataset to create a distribution of cortex volumes. From this distribution, the median adrenal cortex volume for each species was reported and divided by the median cell volume (deer: 1.87 mm³, oldfield: 12.28 mm³) to generate estimates of the total number of cortical cells.

Bulk RNA-seq of adrenal glands and gonads

Adrenal glands were collected from male and female oldfield, beach⁶⁸ (a gift from H. Hoekstra), cloudland deer⁶⁹ (a gift from H. Hoekstra), deer, white-footed and California mice ($n = 8$, 4 of each sex), and deer × oldfield mouse F₁ hybrids ($n = 8$, 4 of each sex). Ovaries and testes were collected from oldfield and deer mice ($n = 8$, 4 of each sex). Tissues were collected following decapitation and immediately flash frozen in dry ice and stored at -70 °C until use.

Frozen adrenals were transferred to Trizol and lysed using a motorized homogenizer (PRO250, Pro Scientific). Total RNA was extracted from the lysate using Direct-zol RNA mini-prep kit (Zymo Research). Following total RNA extraction, Tagmentation-Mediated 3' Sequencing (TM3'-seq)⁷⁰ libraries were created using homebrew Tn5 transposase enzyme⁷¹ for all species except F₁ hybrids. In F₁ hybrids, mRNA was isolated from total RNA using the NEBNext Poly(A) mRNA Magnetic Isolation Kit (New England Biolabs), and then RNA-seq libraries were prepared using the NEBNext Ultra II Directional RNA Library Prep Kit for Illumina (New England Biolabs). Gonad tissue from deer and oldfield mice was homogenized in lysis buffer and mRNA was extracted directly from lysate using the Dynabeads mRNA DIRECT Purification Kit. Libraries were then prepared using the protocol described above.

TM3'-seq libraries were sequenced on an Illumina NextSeq 550 or NextSeq 2000 with single-end reads (1×75 bp) (minimum 1 million (range: 1–5 million) reads per sample). NEBNext libraries from F₁ hybrids were sequenced on an Illumina NextSeq 550 with paired-end reads (2×75 bp) (minimum 12 million (range: 12–21 million) reads per sample). Following sequencing, adapters were trimmed using Trimmomatic v0.36⁷².

To quantify gene expression in tissues from deer, cloudland-deer, beach, and oldfield mice, reads were aligned to the deer mouse genome assembly HU_Pman_2.1.3 (NCBI RefSeq GCF_003704035.1) using STAR v2.6.0a⁷³ in two-pass mode. White-footed mouse libraries were aligned to the *P. leucopus* reference genome UCI_PerLeu_2.1 (NCBI RefSeq GCF_004664715.2), and California mouse libraries were aligned to the *P. californicus insignis* reference genome ASM782708v3 (NCBI RefSeq GCF_007827085.1) before STAR alignment. All these genomes contain a full-length *Akr1c18* annotated gene. Transcript levels were quantified with RSEM v1.3.3⁷⁴. Differentially expressed genes between deer and oldfield mouse adrenals (Benjamini–Hochberg $P_{\text{adjusted}} < 0.05$) were

Article

identified using DESeq2 v1.36.0⁷⁵ after filtering out genes with undetectable or extremely low expression in most samples (TPM ≤ 2 in ≥13 out of 16 adrenals). To quantify allele-specific expression in F₁ hybrid adrenals, reads were pseudoaligned to a hybrid diploid genome of deer and oldfield mouse using kallisto v0.46.0⁷⁶ and allelic expression was quantified using mmseq v1.0.1⁷⁷.

Purification of deer and oldfield mouse AKR1C18 protein

The *Akr1c18* coding sequences of deer and oldfield mice (which are identical) were synthesized, codon optimized for *Escherichia coli*, and cloned into the pET16b plasmid with an N-terminal His-tag followed by a Factor Xa Protease cleavage site by Genscript (Piscataway). The protein was overexpressed in *E. coli* BL21(DE3) at 30 °C for 13 h in the presence of 100 µg ml⁻¹ ampicillin and 1 mM isopropylthio-β-galactoside. The collected cells were resuspended in lysis buffer (50 mM potassium phosphate (pH 7.8), 100 mM NaCl, 10% (v/v) glycerol, 10 mM imidazole, and 2 mM 2-mercaptoethanol) and stored at -80 °C. Recombinant protein was purified using Ni-affinity chromatography. In brief, the resuspended cells were supplemented with 0.1 mg ml⁻¹ DNase and protease inhibitors (Pierce) and kept on ice for 20 min. Cells were lysed by sonication and the lysate was clarified by centrifugation at 47,800g in a Sorvall RC5C centrifuge for 1 h. The clarified lysate was combined with 1 ml Ni-NTA agarose (Invitrogen) and allowed to bind for 2 h. The resin-lysate mixture was poured into a poly-prep column (Bio-Rad), which was washed with 150 ml lysis buffer. AKR1C18 protein was eluted using buffer containing 37.5 mM potassium phosphate pH 7.8, 75 mM NaCl, 7.5% glycerol, 1.5 mM 2-mercaptoethanol, and 250 mM imidazole. The AKR1C18 protein was dialysed against buffer containing 50 mM potassium phosphate pH 7.8, 100 mM NaCl, 10% glycerol, 2.5 mM EDTA, and 2 mM 2-mercaptoethanol. Protein was analysed using SDS-PAGE and was stored at 4 °C, before using it within two weeks.

Progesterone reduction by AKR1C18

The reduction of progesterone was performed as described⁷⁸. See summary in Supplementary Methods.

Adrenal and plasma concentrations of steroid hormones

Mice were left undisturbed in the colony room until time of tissue collection (1–3 pm; Zeitgeber time 10–12), when the cage was quickly moved to an adjacent euthanasia room and overdosed with carbon dioxide inhalation. Then, ~200 µl intracardial blood were obtained from sexually naive deer and oldfield mice. Blood samples were collected within 3 min of moving the cage. Blood was immediately transferred to a tube containing 10 µl 250 mM EDTA and kept on ice until centrifugation. Adrenals were then immediately dissected and flash frozen in dry ice. Blood was centrifuged at 1,500g for 15 min at 4 °C and the plasma supernatant collected. Adrenal glands and plasma were stored at -70 °C until sample processing. Steroids were extracted and quantified as described in Supplementary Methods.

Effect of steroid manipulation on parental care

To quantify parental behaviour in deer and oldfield mice after pharmacological manipulation, 5 mg kg⁻¹ 20α-OHP (Steraloids, Q3600) dissolved in ethanol and then diluted in saline (final concentration 10% ethanol) or vehicle (10% ethanol in saline) was delivered intraperitoneally to sexually naive or experienced parents (60–120 days old) 16–20 h before behaviour testing. This timing allowed for detection of both acute and genomic effects of 20α-OHP delivery and allowed for ample recovery from the stress of handling and injection. To test for acute effects of allo-diol on parental behaviour, 5 mg kg⁻¹ allo-diol (Steraloids, P1950), dissolved in ethanol and then diluted in saline (final concentration 10% ethanol) or vehicle (10% ethanol in saline) was delivered intraperitoneally to 60- to 120-day-old unmated mice or parents with a current litter 1 h before behaviour testing. This short time minimizes the time allo-diol can be metabolized into other compounds.

Mice were transferred to the cage rack adjacent to the testing room 20–24 h before behavioural testing. Each injected mouse was placed individually in a new, clean cage with 0.625 g of compacted nestlet and left undisturbed to habituate for 1 h prior to behaviour testing. Following habituation, the trial begins. The experimenter places one unfamiliar, conspecific pup inside the cage away from the nesting material. After 15 min and again 2 min after that, we added another pup from the same litter to the cage, at least 5 cm from the pup(s) already in the cage. The trial ends after 20 min, after all three pups have been added to the cage. Habituation and behaviour testing occurred in the dark under 870 nm infrared LED lighting between Zeitgeber time 6–16.

Pups were used for behaviour testing between postnatal days 2–6, an age in which they cannot return to the nest without assistance. Between behaviour trials, pups were kept in an incubator at 37 °C; at the end of testing, each litter was returned to their parental cage and observed to ensure that they were licked and/or retrieved by a parent.

Behaviour trials were video recorded using two Raspberry Pi 3 computers with NoIR Camera Modules to record the mice in their cage from two different angles (top and side). Video footage from both angles was analysed blind to the treatment each mouse received. For the first 15 min of the trial, the duration of time the test mouse spent huddling over the pup and time spent grooming or licking the pup were calculated. The proportion of pups retrieved (out of three pups added to the cage over the 20-min trial) was also scored. Nest quality at the end of the 20-min trial was scored on a 4-point scale described²². In the rare event of a pup attack (the test individual bites the pup), we immediately stopped the assay, removed the pup, and did not reuse that pup in subsequent trials. In deer mouse mothers, there was a high rate of infanticide even after injection with vehicle, which prohibited testing the effects of 20α-OHP on parental behaviour (see Extended Data Fig. 2d).

Effect of 20α-OHP on pair bonding

To quantify pair bonding (preference for huddling with the partner over a stranger) in deer and oldfield mice after pharmacological manipulation, 5 mg kg⁻¹ 20α-OHP (Steraloids, Q3600) or vehicle was delivered to males and females of established breeding pairs (at least 2 litters together) 16–20 h before behaviour testing.

Mice were transferred to the cage rack adjacent to the testing room three days before behavioural testing. Each mouse was assigned a novel mouse of the same species and opposite sex. Focal mice were habituated in their home cage and novel mice were habituated in the cage of a different established breeding pair for 20 min per day for 2 days prior to the test. On test day, each focal mouse was habituated to their home cage without nesting material for 20 min, and then the test mouse (partner or novel opposite sex mouse) was added and left undisturbed for 1 h. Behaviour testing occurred in the dark under 870 nm infrared LED lighting between Zeitgeber time 6–16 and recorded as described for the parental behaviour experiments. Huddling (defined by side-by-side contact with or without grooming) during the first 10 min of the trial was recorded using BORIS⁷⁹ by an experimenter blind to the treatment each mouse received.

Effect of 20α-OHP on elevated plus maze behaviour

The elevated plus maze apparatus contained two closed arms and two open arms (12 inch long and 2 inch wide; wall height: 17.5 inch) made from acrylic. The open arms were lined with a 0.25-inch acrylic ledge to discourage mice from falling or jumping off the apparatus. The platform was 24 inch from the ground and brightly illuminated with white LED strip lights affixed to the ceiling. Before each trial, the subject was transferred from its home cage to a 5 × 3.5 × 1.5 inch acrylic box, and the box was placed in the elevated plus maze for a 2-min acclimatization period. After 2 min, the box was opened at the centre of the maze without disturbing the mouse. After release from the acclimation box, the trial begins, and the subject is recorded exploring the elevated

plus maze using a Raspberry Pi camera for 5 min. The centroid position of the mouse was tracked using a custom Python script adapted from Behavior Analysis Software (<https://you.stonybrook.edu/mckinnonrosati/behavior-analysis-software/>), and duration spent in the closed and open arms was calculated. If a mouse climbed or jumped off of the elevated plus maze, the mouse was retrieved and returned to the acclimatization box for 2 min, and the trial began again. Mice that jumped off the apparatus more than once were discarded from further analysis. All surfaces of the elevated plus maze were cleaned with 70% ethanol between trials.

Metabolism of 20 α -OHP by deer and oldfield brain tissue

Deer and oldfield mice were rapidly sacrificed by cervical dislocation, and then the cerebellum and hypothalamus were dissected and kept on ice. Half of the cerebellum and hypothalamus were then minced into 1-mm pieces and split evenly into vials containing 200 μ l Medium 199 (Gibco 12340030) with 2.5 μ l 20 α -OHP (1 μ M final) dissolved in ethanol or 200 μ l Medium 199 with 2.5 μ l ethanol (vehicle). Vials were incubated at 37 °C in 95% O₂ and 5% CO₂ for 2 h with periodic shaking. After incubation, samples were centrifuged at max speed for 3 min at 4 °C, and the supernatant was discarded. The tissue pellet was stored at -70 °C until steroids were extracted. Progesterone, allo-diol, and allopregnanolone were quantified as described in Supplementary Methods.

Recording tonic and phasic GABAergic currents

Sagittal slices were prepared from 6- to 12-week-old *P. polionotus* following ref. 33. Tonic currents were recorded from cerebellar granule cells at ~32 °C with an internal solution containing (in mM) 110 CsCl, 10 caesium gluconate, 10 HEPES, 10 Mg-ATP, 0.5 Na-GTP, 5 phosphocreatine-di(tris), and 5 phosphocreatine-disodium, and 0.1 Alexa 594, pH adjusted to 7.2 with CsOH, osmolality adjusted to 310 mOsm kg⁻¹. The reversal potential for chloride was adjusted to -0 mV to maximize GABAergic current amplitude at -60 mV holding potential. Visually guided whole-cell recordings were obtained with patch pipettes of ~3–5 M Ω resistance pulled from borosilicate capillary glass (BF150-86-10, Sutter Instrument). Electrophysiology data was acquired using a Sutter dPatch amplifier (Sutter Instruments), digitized at 10 kHz and filtered at 5 kHz. For isolating inhibitory currents in voltage clamp the following receptor antagonists were added to the bath solution (in μ M): 2 R-CPP, 5 NBQX, 1 strychnine, 1.5 CGP to block NMDA, AMPA, glycine and GABA_A receptors. GABAergic currents were blocked with 50 μ M gabazine (SR95531). All drugs were purchased from Abcam and Tocris. Allo-diol and 20 α -OHP (P1950, Q3600, Steraloids) were dissolved in ethanol at a stock concentration of 10 mg ml⁻¹ and used at a final concentration of 300 nM during bath application. THIP was used at a concentration of 500 nM, in the absence or in the presence of 300 nM allo-diol or 20 α -OHP. Drugs were allowed to wash on for 10 min to ensure full equilibration. After each experiment, the tubing and recording chamber were rinsed with ethanol followed by distilled water for 10 min to remove lipophilic drugs.

Electrophysiology data were analysed using AxographX and IgorPro (Wavemetrics). Tonic current amplitude was determined by generating all-points histograms of continuously recorded current under control conditions, in the presence of steroid and with gabazine. The histograms were fit with a Gaussian, yielding the mean current⁸⁰. For all recordings, a 10 mV 500 ms test pulse was recorded before and after all drug application to assess the effect of drug application on membrane resistance (input resistance R_i) and stability of throughout the recording (serial resistance R_s). Cells were rejected if R_s changed by >15% over the duration of the recording.

snRNA-seq of adrenal glands

Adrenal glands were collected following decapitation and flash frozen in dry ice for the following 6 conditions: 3 species (deer, oldfield or

C57BL/6J *M. musculus* laboratory mice, unmated -60 days old) × 2 sexes, with adrenals from 3 mice pooled per treatment. Nuclei were extracted using the Chromium Nuclei Isolation Kit with RNase Inhibitor (10X Genomics), and nuclei concentration and quality was determined with trypan blue staining on a haemocytometer. Nuclei from all treatments were clump-free with minimal debris and minimal blebbing, indicating high quality nuclei preparations. Nuclei suspensions were loaded onto a Chromium Chip G (one treatment per reaction), and GEMs were generated using the Chromium Controller (10X Genomics). Libraries were created using the Chromium Next GEM Single Cell 3' Kit v3.1 and then sequenced on an Illumina NextSeq 2000 with an insert size of 90 bp.

Peromyscus reads were aligned to the *P. maniculatus* genome *HU_Pman_2.1.3* (NCBI RefSeq GCF_003704035.1) and C57BL/6J reads were aligned to the GRCm39 genome assembly (NCBI RefSeq GCF_000001635.27) using 10X Genomics CellRanger v7.1 and feature-barcode matrices were generated. Ambient RNA was removed in silico by CellBender v0.3.0⁸¹, and gene expression matrices were then analysed in Seurat v4.3.0⁸². First, low-quality cells and likely multiplets were discarded. Multiplets were detected using Vireo⁸³ and subsequently removed; additionally, cells containing fewer than 200 unique feature counts, more than 2,500 unique feature counts, or more than 3% mitochondrial gene counts were removed. After filtering, there were 8,013–11,444 cells across *Peromyscus* treatments (2 species × 2 sexes), containing a mean of 1,589–2,472 unique molecular identifiers (UMIs) per cell and a mean of 936–1,276 unique features per cell. The number of *M. musculus* cells was 11,553 in males (812 mean UMIs and 639 mean features per cell) and 21,512 in females (1,134 mean UMIs and 848 mean features per cell).

Datasets from deer mice and oldfield mice were then integrated. In brief, anchors for dataset integration were identified using a reciprocal principal components analysis (rPCA), in which the deer mouse dataset is projected onto the reduced PCA space of the oldfield mouse data and vice versa, with 1,800 anchor features and 20 PCA dimensions⁸⁴. The strength of integration was increased by setting the k.anchor parameter to 20 to ensure that homologous cell types aligned between species. Clusters were identified in Seurat using the FindClusters() function with a cluster resolution parameter of 0.3. Upregulated differentially expressed genes (that is, markers) of the zona inaudita cell type were determined using the FindMarkers() Seurat function comparing all cells of the zona inaudita cluster to all other cell types in deer and oldfield mice. Zona inaudita markers had an adjusted *P* value < 0.05 of differential expression against all other cell clusters and surpassed a log₂ fold change threshold of 1. Gene ontology (GO) term enrichment analysis was performed using PANTHER⁸⁵.

To compare cell-type homology between *Peromyscus* and *M. musculus*, deer mouse and oldfield mouse datasets were integrated with C57BL/6J data after filtering the included features to the set of 16,411 one-to-one orthologues shared between the deer mouse and C57BL/6J genome annotations (Supplementary Table 2), which were inferred using TOGA⁸⁶. Integration and clustering was performed as described above.

F₂ adrenal RNA-seq

F₂ hybrids of deer mice and oldfield mice were generated from a founding population of four deer mouse mothers and four oldfield mouse fathers²². The adrenals of 706 adult F₂ hybrids were dissected and stored at -70 °C. Adrenals were lysed using a motorized homogenizer in lysis buffer and mRNA was extracted using Dynabeads mRNA DIRECT Purification Kit. Following mRNA extraction, TM3'-seq⁷⁰ libraries were created using homebrew Tn5 transposase enzyme⁷¹. Adrenal transcriptomes were sequenced using 1 × 76 bp reads on an Illumina NextSeq 550 to an average depth of 3.3 million reads (minimum 2 million reads per sample). Reads were adapter trimmed, aligned, and quantified as described in 'Bulk RNA-seq of adrenal glands and gonads'.

eQTL mapping in F₂ hybrids

Genome-wide ancestry (deer mouse, oldfield mouse or heterozygous) for each F₂ mouse was determined from ddRAD-sequencing for 706 F₂ hybrid mice (369 male, 337 female) mapped to the deer mouse HU_Pman2.1.3 reference genome. A hidden Markov model (Ancestry-HMM⁸⁷) was used to calculate genotype probabilities along each chromosome from the number of reads mapping to the deer mouse versus the oldfield mouse single nucleotide polymorphism at each fixed variant position. The position of fixed single nucleotide polymorphisms were determined from publicly available whole-genome sequences from both species obtained from the NCBI short-read archive.

Genotype probabilities were imported into R/qt1⁸⁸ using read.cross.msg.1.5.R (https://github.com/dstern/read_cross_msg/) and QTL mapping of zona inaudita gene expression (transcripts per million of each marker gene) was conducted for males and females separately using scanone under a nonparametric model. The heatmap of zona inaudita marker gene expression was created using pheatmap v1.0.12 (<https://github.com/raivokolde/pheatmap>). To calculate the module scores, the expression of each gene in the TF and the ECM modules was first z-scored across individuals and then the z-score of each gene in that module in an individual were averaged. To perform mediation analyses, QTL mapping was performed using scanone under a parametric model with the log-transformed gene expression of *Gadd45a* or *Tnn* as an additive covariate. The scanone function was also used to compute the genome-wide LOD significance threshold at $\alpha < 0.05$ using 1,000 permutations. Data were plotted in R version 4.2.1 using ggplot2 v3.4.0⁸⁹.

Reporting summary

Further information on research design is available in the Nature Portfolio Reporting Summary linked to this article.

Data availability

Sequence data are available at NCBI Sequence Read Archive under BioProject ID PRJNA1094591. Source data are provided with this paper.

65. Choi, H. M. T. et al. Third-generation in situ hybridization chain reaction: multiplexed, quantitative, sensitive, versatile, robust. *Development* **145**, dev165753 (2018).
66. Kuehn, E. et al. Segment number threshold determines juvenile onset of germline cluster expansion in *Platynereis dumerilii*. *J. Exp. Zool. B* **338**, 225–240 (2022).
67. Renier, N. et al. iDISCO: A simple, rapid method to immunolabel large tissue samples for volume imaging. *Cell* **159**, 896–910 (2014).
68. Bedford, N. L. et al. Automated tracking reveals the social network of beach mice and their burrows. Preprint at *bioRxiv* <https://doi.org/10.1101/2021.08.07.455531> (2021).
69. Kingsley, E. P., Kozak, K. M., Pfeifer, S. P., Yang, D.-S. & Hoekstra, H. E. The ultimate and proximate mechanisms driving the evolution of long tails in forest deer mice. *Evolution* **71**, 261–273 (2017).
70. Pallares, L. F., Picard, S. & Ayroles, J. F. TM3seq: a fragmentation-mediated 3' sequencing approach for improving scalability of RNA-seq experiments. *G3* **10**, 143–150 (2020).
71. Picelli, S. et al. Tn5 transposase and fragmentation procedures for massively scaled sequencing projects. *Genome Res.* **24**, 2033–2040 (2014).
72. Bolger, A. M., Lohse, M. & Usadel, B. Trimmomatic: a flexible trimmer for Illumina sequence data. *Bioinformatics* **30**, 2114–2120 (2014).
73. Dobin, A. et al. STAR: ultrafast universal RNA-seq aligner. *Bioinformatics* **29**, 15–21 (2013).
74. Li, B. & Dewey, C. N. RSEM: accurate transcript quantification from RNA-seq data with or without a reference genome. *BMC Bioinformatics* **12**, 323 (2011).

75. Love, M. I., Huber, W. & Anders, S. Moderated estimation of fold change and dispersion for RNA-seq data with DESeq2. *Genome Biol.* **15**, 550 (2014).
76. Bray, N. L., Pimentel, H., Melsted, P. & Pachter, L. Near-optimal probabilistic RNA-seq quantification. *Nat. Biotechnol.* **34**, 525–527 (2016).
77. Turro, E. et al. Haplotype and isoform specific expression estimation using multi-mapping RNA-seq reads. *Genome Biol.* **12**, R13 (2011).
78. Detlefsen, A. J., Wangtrakuldee, P. & Penning, T. M. Characterization of the major single nucleotide polymorphic variants of aldo-keto reductase 1C3 (type 5 17 β -hydroxysteroid dehydrogenase). *J. Steroid Biochem. Mol. Biol.* **221**, 106121 (2022).
79. Friard, O. & Gamba, M. BORIS: a free, versatile open-source event-logging software for video/audio coding and live observations. *Methods Ecol. Evol.* **7**, 1325–1330 (2016).
80. Bright, D. P. & Smart, T. G. Methods for recording and measuring tonic GABA_A receptor-mediated inhibition. *Front. Neural Circuits* **7**, 193 (2013).
81. Fleming, S. J. et al. Unsupervised removal of systematic background noise from droplet-based single-cell experiments using CellBender. *Nat. Methods* **20**, 1323–1335 (2023).
82. Hao, Y. et al. Integrated analysis of multimodal single-cell data. *Cell* **184**, 3573–3587.e29 (2021).
83. Huang, Y., McCarthy, D. J. & Stegle, O. Vireo: Bayesian demultiplexing of pooled single-cell RNA-seq data without genotype reference. *Genome Biol.* **20**, 273 (2019).
84. Hao, Y. et al. Dictionary learning for integrative, multimodal and scalable single-cell analysis. *Nat. Biotechnol.* **42**, 293–304 (2023).
85. Mi, H. et al. Protocol update for large-scale genome and gene function analysis with the PANTHER classification system (v14.0). *Nat. Protoc.* **14**, 703–721 (2019).
86. Kirilenko, B. M. et al. Integrating gene annotation with orthology inference at scale. *Science* **380**, eabn3107 (2023).
87. Corbett-Detig, R. & Nielsen, R. A hidden Markov model approach for simultaneously estimating local ancestry and admixture time using next generation sequence data in samples of arbitrary ploidy. *PLoS Genet.* **13**, e1006529 (2017).
88. Bromman, K. W., Wu, H., Sen, S. & Churchill, G. A. R/qt1: QTL mapping in experimental crosses. *Bioinformatics* **19**, 889–890 (2003).
89. Wickham, H. *Ggplot2: Elegant Graphics for Data Analysis* (Springer-Verlag, 2016).

Acknowledgements This work was supported by the following grants: Searle Scholarship, Klingenstein-Simons Fellowship in Neuroscience, Sloan Foundation Fellowship, and National Institutes of Health (NIH) R00HD084732, R21HD106241 and R35GM143051 to A.B.; the Simons Society of Fellows Junior Fellowship 855220 to J.R.M.; Canadian Institutes of Health Research Project Grant 4226405 to K.K.S.; Tishman Fellowship to S.L.; and SFARI Bridge to Independence award and Rose F. Kennedy Intellectual and Developmental Disabilities Research Center pilot grant to S.R. Imaging was performed with support from the Zuckerman Institute's Cellular Imaging platform, which received grant S10OD023587-01 from the NIH. Columbia University's Shared Research Computing Facility, where computations were performed, was supported by NIH grant G20RR030893-01 and NYSTAR contract C090171. L. Hammond and H. Ibarra provided training and advice on microscope imaging. C. Zhang shared reagents. L. Remedio shared reagents and advice on tissue clearing. H. Pan and M. Hiller helped run TOGA to find orthologues. H. Hoeckstra provided beach mice and cloudland mice adrenals. M. Tosches, R. Axel, S. Siegelbaum and D. Bambah-Mukku and his students provided comments on the manuscript. C. Everett created the diagram in Fig. 4f. Schematics in Fig. 2a,i and Extended Data Fig. 3 were created using BioRender.com.

Author contributions N.N. and A.B. conceived and designed the study. N.N. conducted all transcriptomic and genetic experiments and analyses, with contribution from M.U. and J.R.M. J.R.M. performed behaviour assays with contributions from V.S.E., I.B.B., K.H., M.U. and N.N. N.N. and M.U. performed adrenal histology. N.N. and E.L. characterized adrenal mass and volume. K.H. developed the pair-bonding assay. C.G. and J.R.M. built behaviour testing apparatus. S.A.W. performed AKR1C18 biochemistry experiments. K.K.S. and A.P. developed LC-MS/MS steroid quantification methods and quantified steroid levels. S.R. and S.L. conducted electrophysiology experiments and analysis. N.N., J.R.M. and A.B. wrote the paper with input from all authors.

Competing interests The authors declare no competing interests.

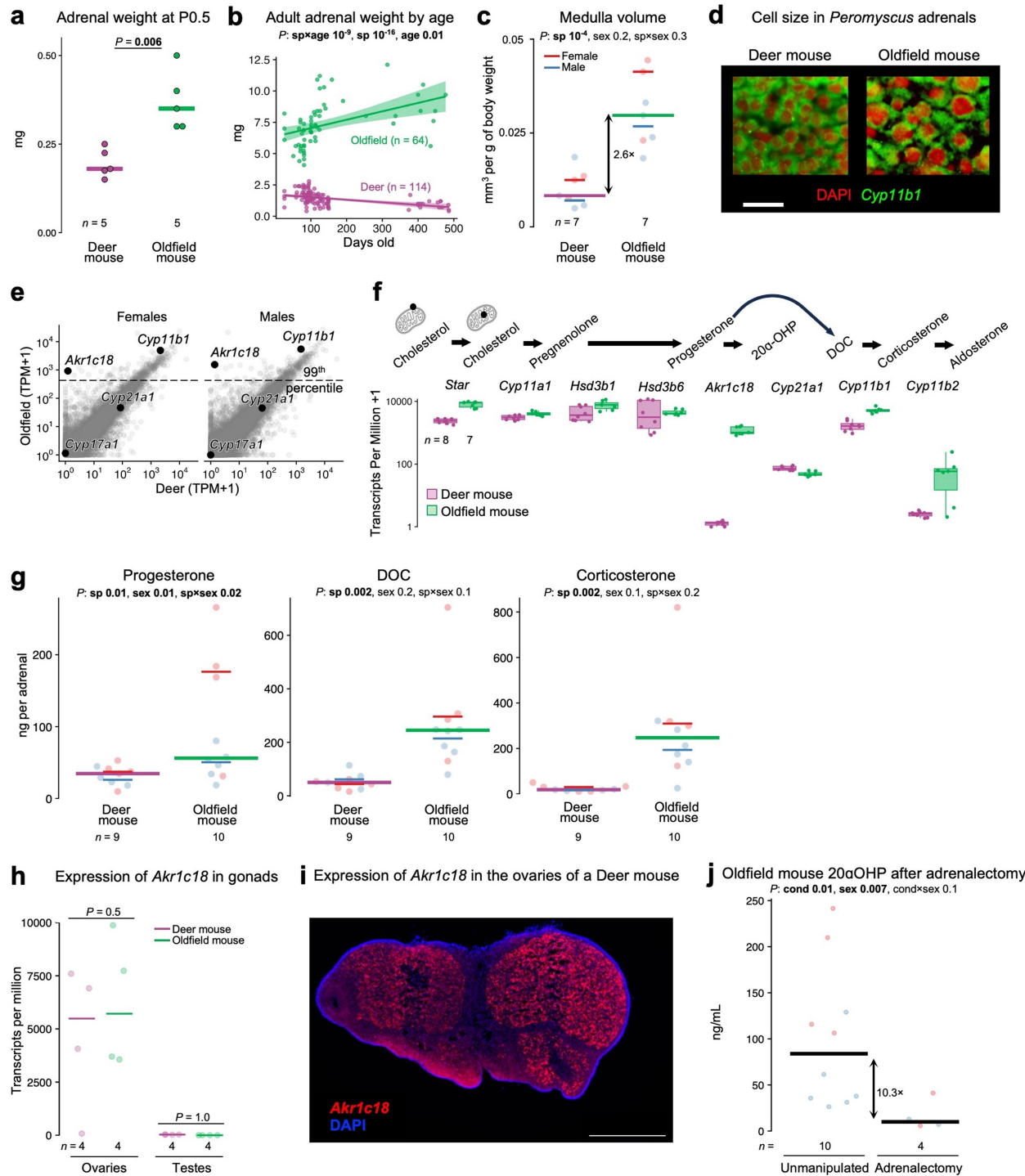
Additional information

Supplementary information The online version contains supplementary material available at <https://doi.org/10.1038/s41586-024-07423-y>.

Correspondence and requests for materials should be addressed to Andres Bendesky.

Peer review information *Nature* thanks Tali Kimchi and Jessica Tollkuhn for their contribution to the peer review of this work. Peer reviewer reports are available.

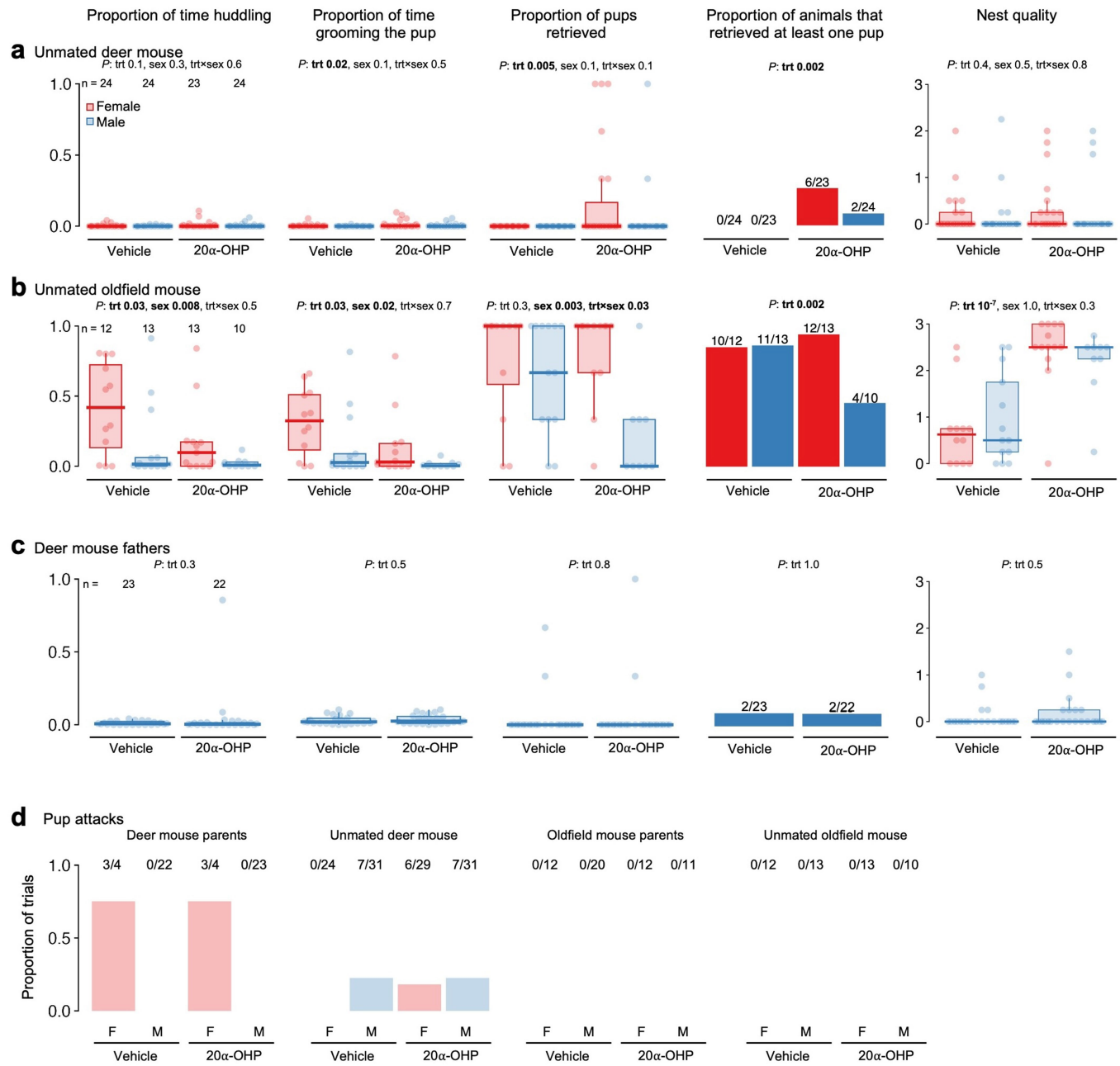
Reprints and permissions information is available at <http://www.nature.com/reprints>.



Extended Data Fig. 1 | Anatomical, molecular, and biochemical characterization of deer- and oldfield adrenal glands. **a**, Adrenal weight at postnatal day 0.5. Lines at median. **b**, Adult adrenal weight by age. *P*-values by generalized linear model. Band is 95% confidence interval. **c**, Adrenal medulla volume. Lines at median. *P*-values by generalized linear model. **d**, Representative adrenal section from the zona fasciculata (zF) of the deer- and oldfield mouse adrenal cortex. *Cyp11b1* (green) labeled by *in situ* hybridization and counterstained with DAPI (red). Five independent biological replicates per species yielded similar results. Scale bar, 20 μ m. **e**, Scatterplot of gene expression by species and sex. **f**, Boxplots of the expression of steroidogenic enzymes in

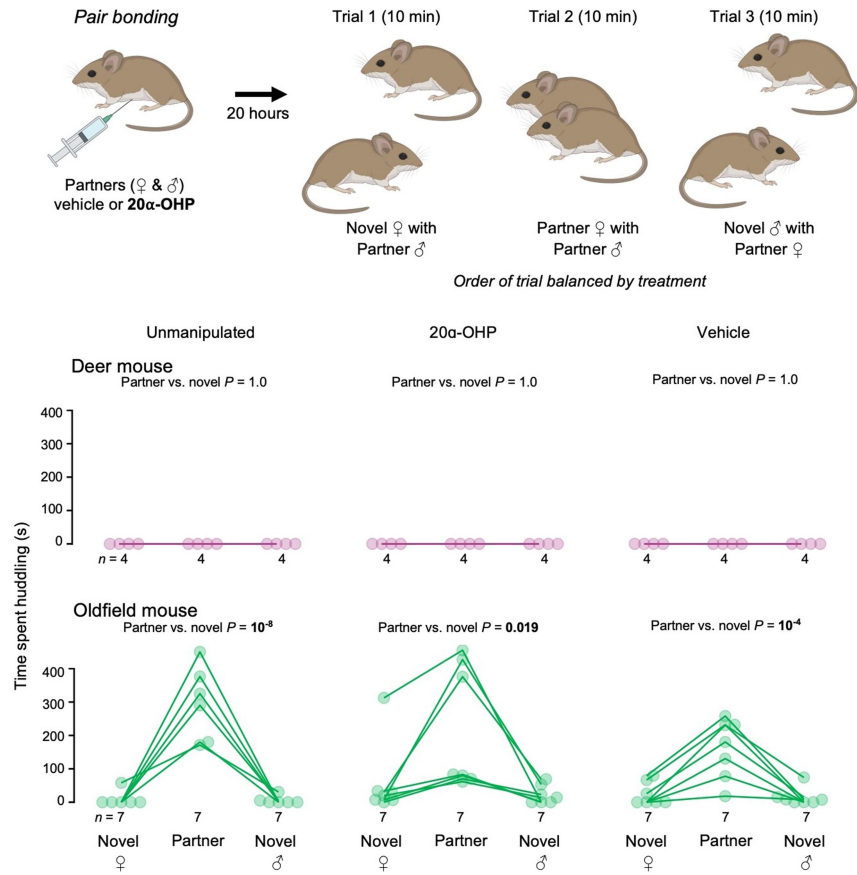
the corticosterone- and 20 α -OHP synthesis pathways in the adrenal. Boxplot hinges are 25th and 75th quartiles, whiskers are 1.5 \times interquartile range, line at median. **g**, Total steroid levels in the adrenal gland of deer and oldfield mice. Lines at median. *P*-values by generalized linear model. DOC, deoxycorticosterone. **h**, Expression of *Akr1c18* in the ovaries and testes of oldfield and deer mice. Lines at median. *P*-values by two-sided *t*-test. **i**, *Akr1c18* (red) labeled by *in situ* hybridization in the ovary of a deer mouse and counterstained with DAPI (blue). Three independent biological replicates per species yielded similar results. Scale bar, 0.5 mm. **j**, Circulating 20 α -OHP levels in the blood of oldfield mice after adrenalectomy. Lines at median. *P*-values by generalized linear model.

Article

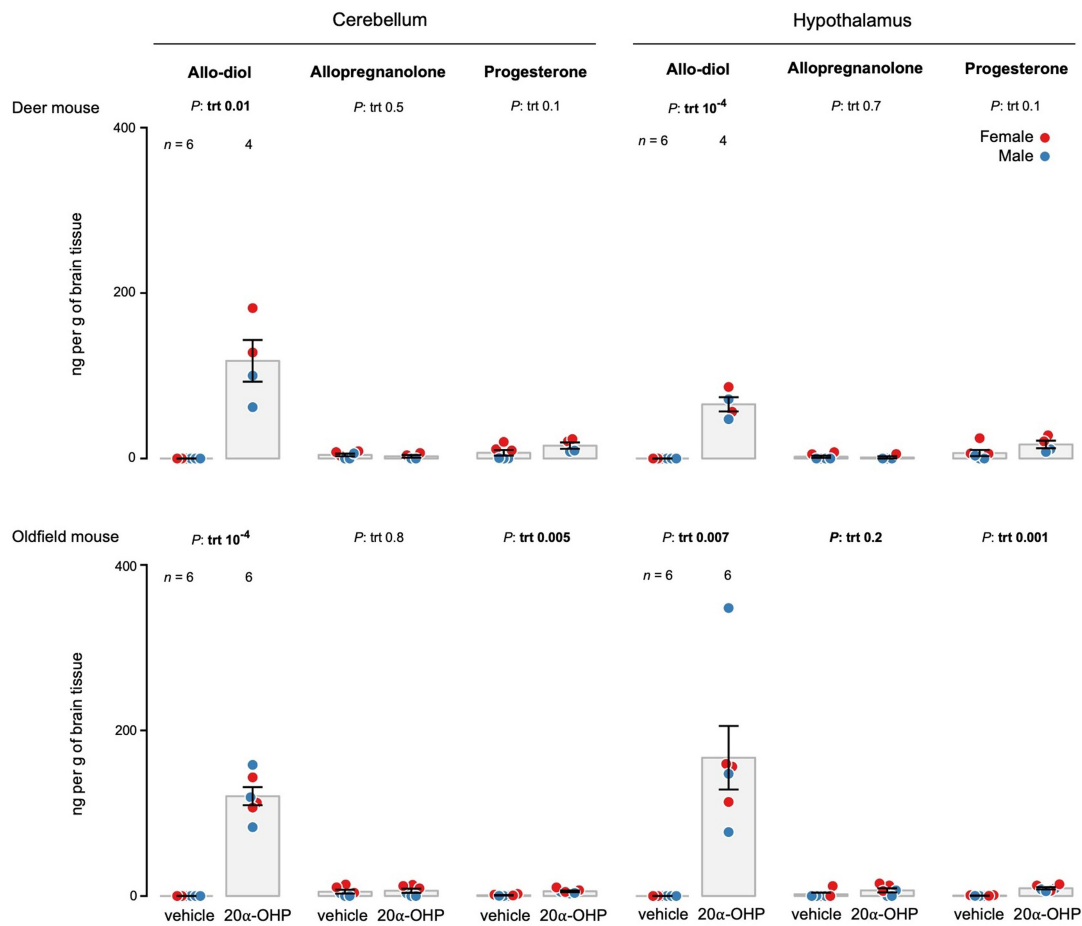


Extended Data Fig. 2 | Effects of 20 α -OHP on alloparental and parental care. Male and female care for pups as measured by proportion of time spent huddling pups, proportion of time spent grooming pups, fraction of pups retrieved to the nest, and nest quality score (from 0 to 4) in **a**, unmated deer mice, **b**, unmated oldfield mice, and **c**, deer mouse fathers. Boxplot hinges are 25th and 75th quartiles, whiskers are 1.5 \times interquartile range, line at median.

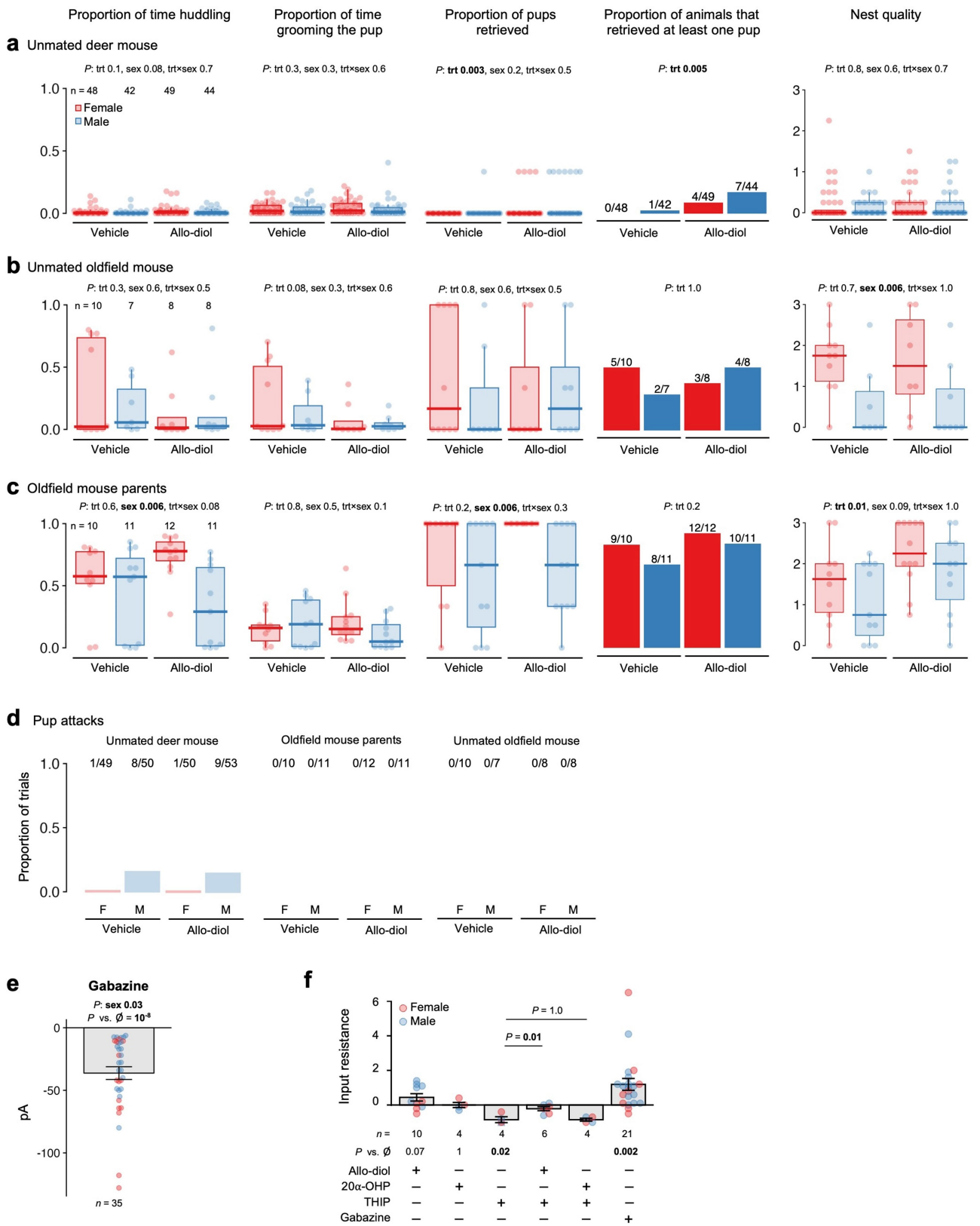
P-values by generalized linear model for proportion of time huddling, proportion of time grooming the pup, proportion of pups retrieved, and nest quality. P-values for proportion of animals that retrieved at least one pup by Fisher's exact test. **d**, Proportion of pup attacks by species, treatment, and reproductive experience.



Extended Data Fig. 3 | Partner preference is not affected by $20\alpha\text{-OHP}$. Top: Schematic of the experimental design of the partner preference test. Bottom: Observations from the same breeding pairs are connected by lines (10 min partner preference test). P -values by generalized linear model (effect of trial type).



Extended Data Fig. 4 | 20 α -OHP is converted to allo-diol in the brain of deer- and oldfield mice. a, Concentration of allo-diol, allopregnanolone and progesterone in deer- and oldfield mouse cerebellum and hypothalamus after incubation with 20 α -OHP, as measured by LC-MS/MS. P -values by two-sided t -test.

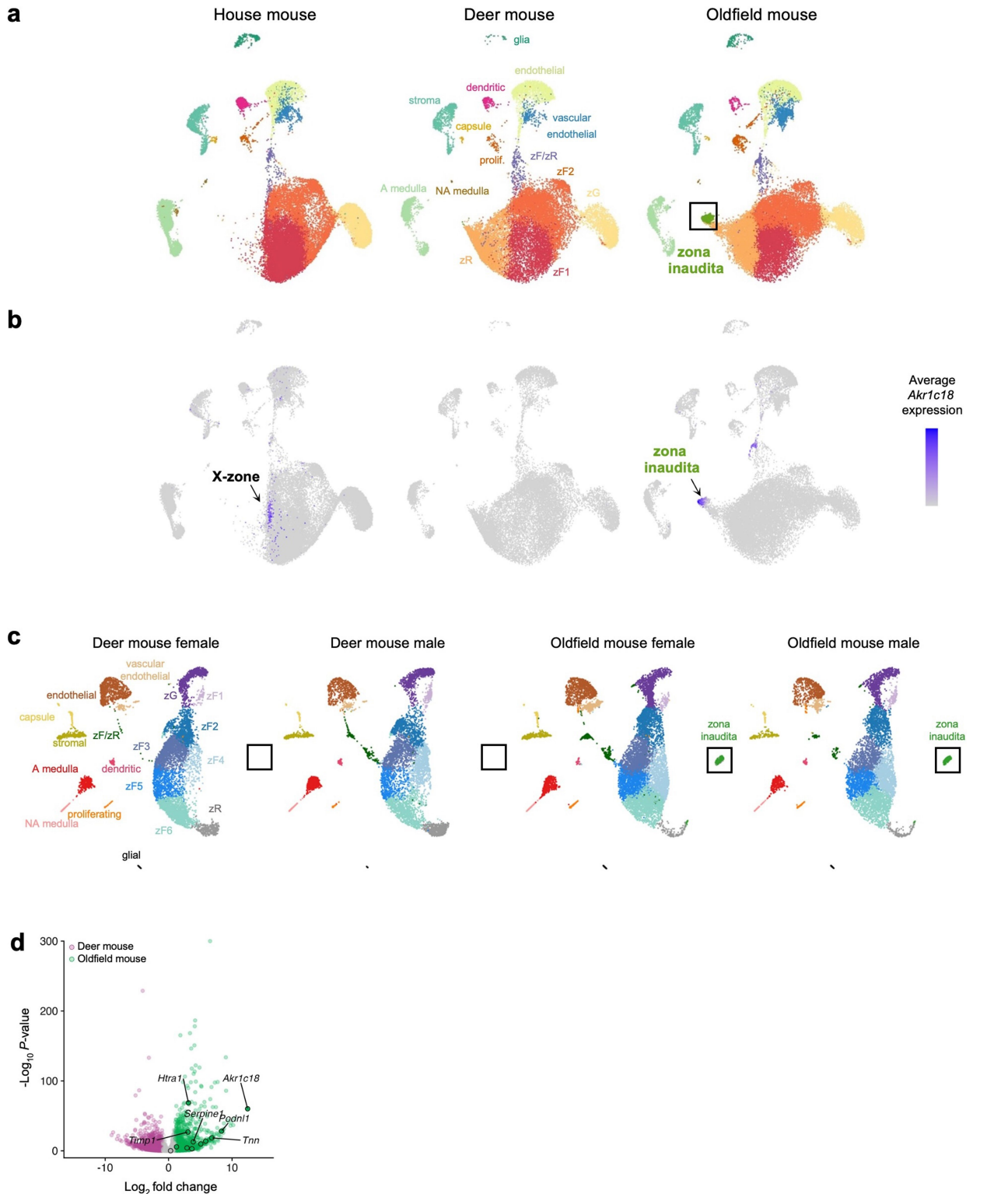


Extended Data Fig. 5 | See next page for caption.

Article

Extended Data Fig. 5 | Effects of allo-diol on alloparental and parental care, and on $\delta\text{GABA}_A\text{R}$. Male and female care for pups as measured by proportion of time spent huddling pups, proportion of time spent grooming pups, fraction of pups retrieved to the nest, and nest quality score in **a**, unmated deer mice, **b**, unmated oldfield mice, and **c**, oldfield parents. Boxplot hinges are 25th and 75th quartiles, whiskers are 1.5 \times interquartile range, line at median. *P*-values by generalized linear model for proportion of time huddling, proportion of time grooming the pup, proportion of pups retrieved, and nest quality. *P*-values for proportion of animals that retrieved at least one pup by Fisher's exact test.

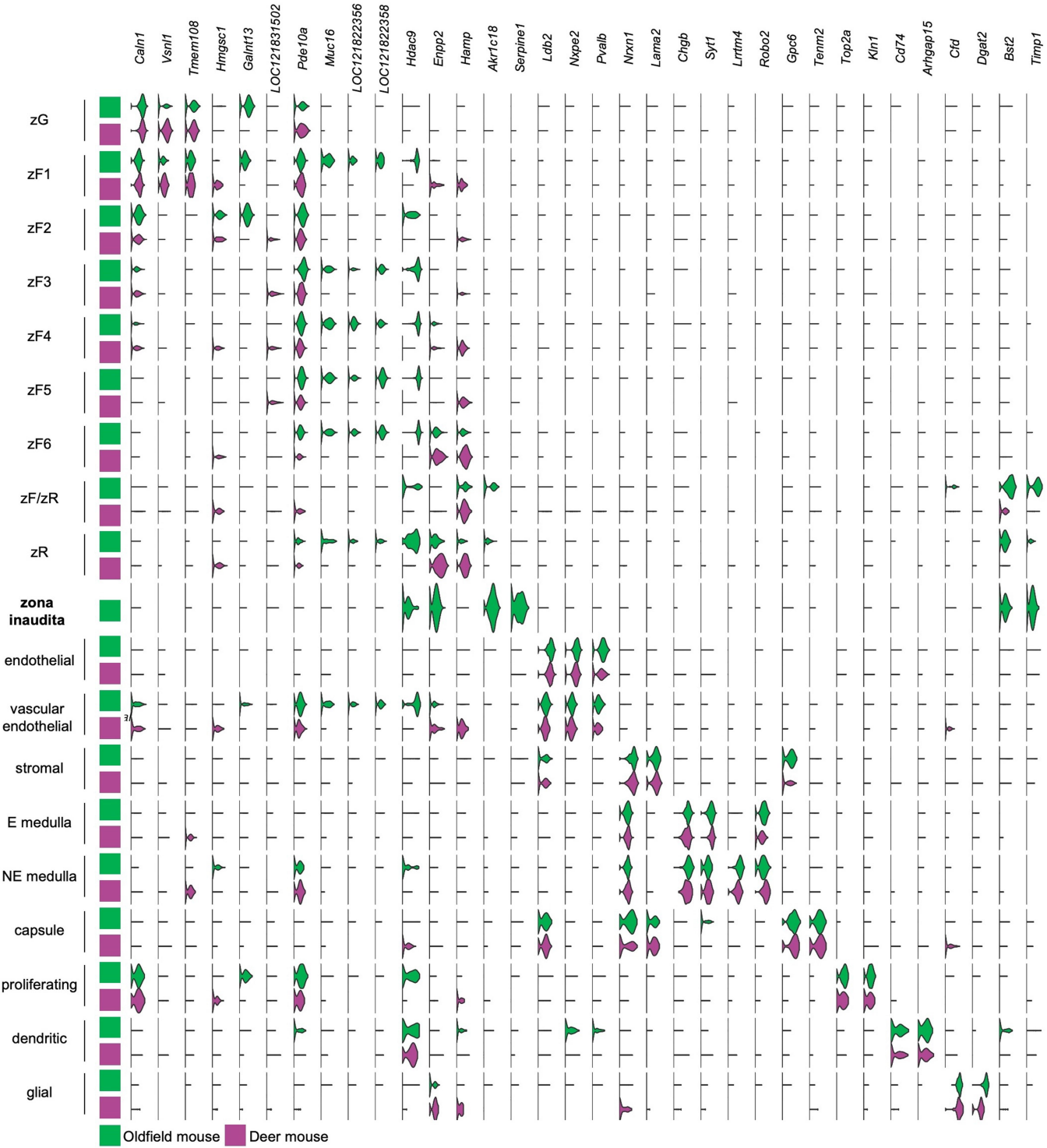
d, Proportion of pup attacks by species, treatment, and reproductive experience. **e**, Baseline tonic GABA receptor currents with leak current subtracted, after gabazine application. **f**, Input resistance (R_i) under different pharmacological conditions. No change in R_i in the presence of allo-diol and 20 α -OHP suggests no effect on GABA receptor currents. A decrease in R_i in the presence of THIP is consistent with an increase in GABA receptor currents. This effect is diminished when THIP is co-applied with allo-diol but not with 20 α -OHP. R_i increases in gabazine when all GABA receptors are blocked. *P*-values by two-sided one-sample *t*-test ($\mu = 0$) and two-sample two-sided *t*-tests. Bars denote the mean \pm SEM.



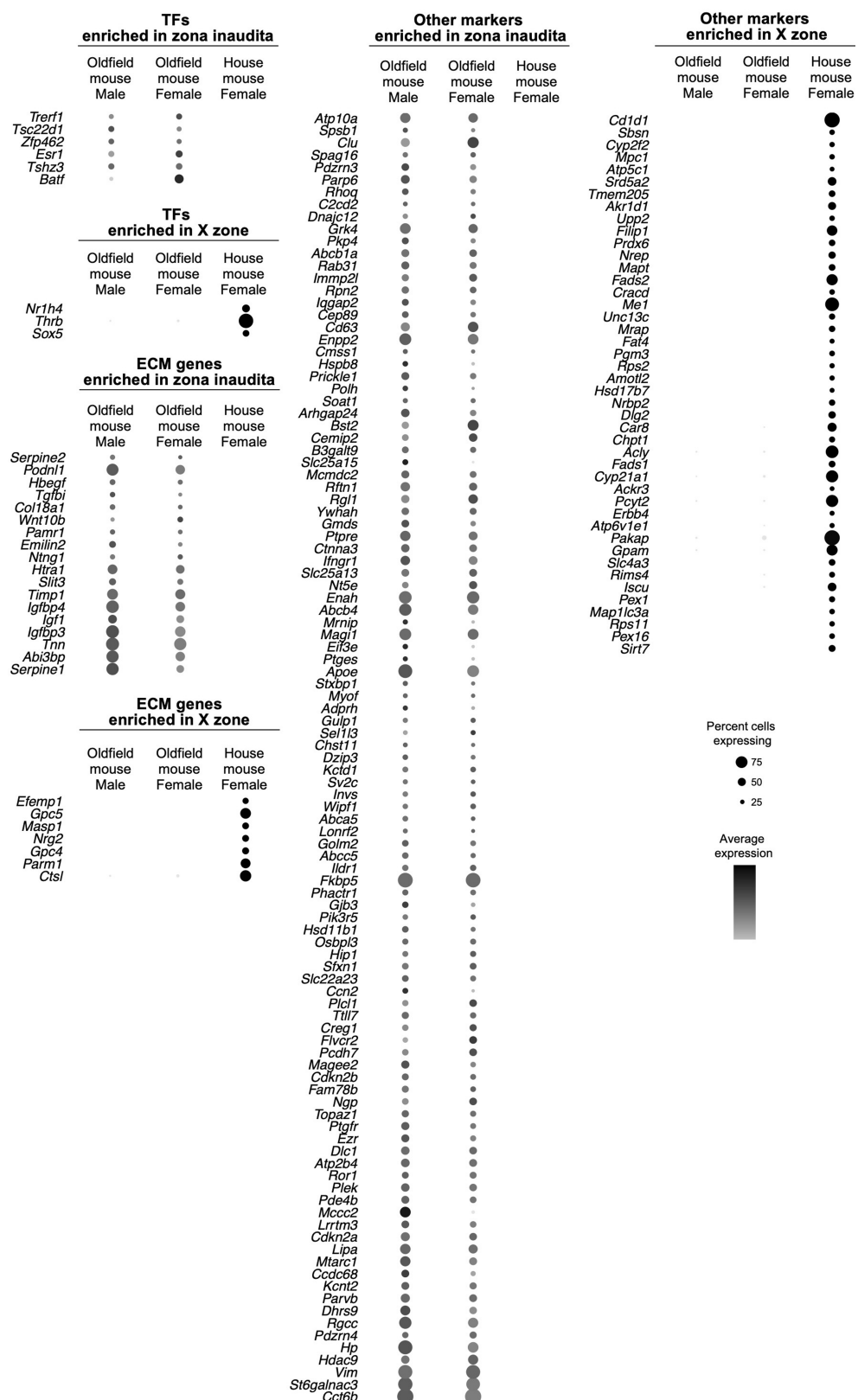
Extended Data Fig. 6 | UMAP visualization of the house-, deer-, and oldfield mouse adrenal. **a**, UMAP of integrated analysis of house mouse, deer mouse, and oldfield mouse adrenal nuclei. **b**, UMAP showing *Akr1c18* expression in adrenal cells, marking the X zone in house mice and the zona inaudita in oldfield mice. **c**, UMAP of integrated analysis of deer mouse and oldfield mouse nuclei,

then split by sex. **d**, Volcano plot of differential adrenal gene expression between deer- and oldfield mouse (purple: higher in deer mouse, green: higher in oldfield mouse, grey: n.s.). *Akr1c18* and extracellular matrix gene markers of the zona inaudita (from Fig. 3g) are highlighted. False Discovery Rate=0.05. A medulla, adrenergic medulla; NA medulla, noradrenergic medulla.

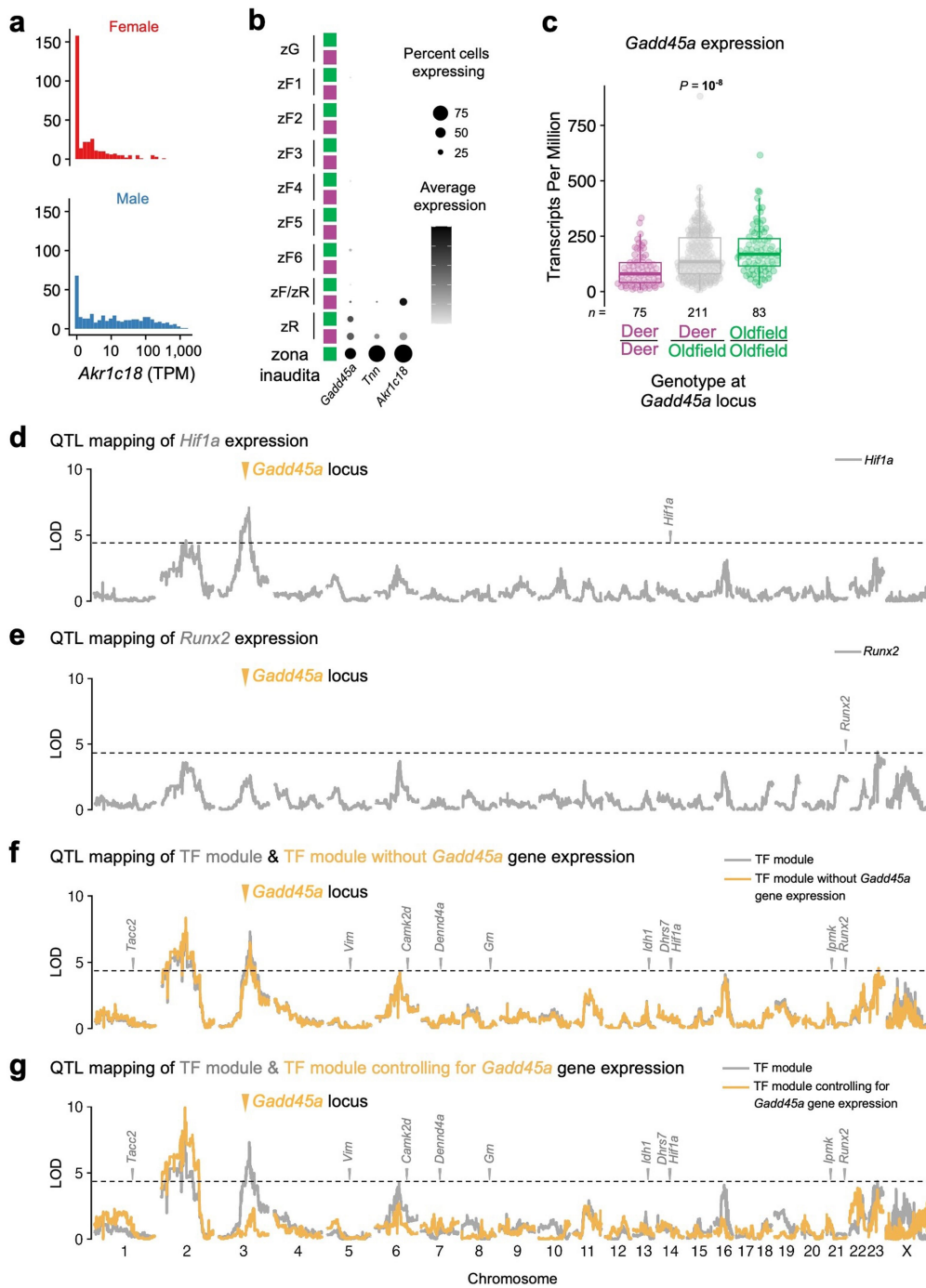
Article



Extended Data Fig. 7 | Expression of top marker genes of the adrenal zones of deer mice and oldfield mice. Violin plots denoting the top two markers of each adrenal cell type.

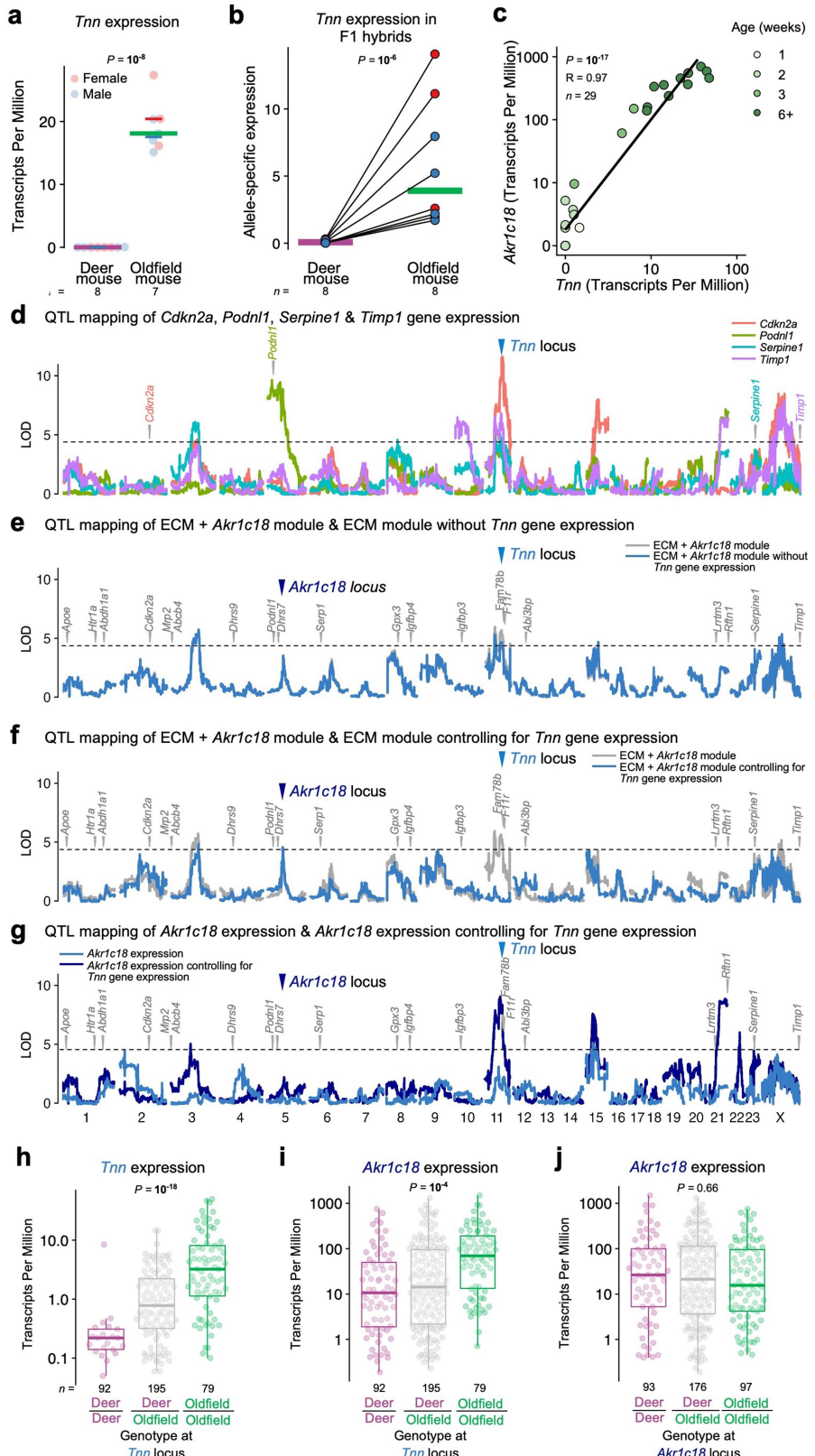


Extended Data Fig. 8 | Dot plots of marker genes of the zona inaudita of oldfield mice and the X zone of house mice. Expression of transcription factors (TFs), extracellular matrix (ECM) genes, and other genes upregulated in the zona inaudita or X zone. Note that in adults, the X zone is only present in unmated females.



Extended Data Fig. 9 | Cis-regulation of *Gadd45a* contributes to transcription factor module expression. **a**, Expression of *Akr1c18* in the adrenal of female and male deer × oldfield F₂ hybrids. **b**, Dot plot of *Gadd45a*, *Tnn*, and *Akr1c18* expression in adrenal cortex cell types. **c**, *Gadd45a* expression by genotype at the *Gadd45a* locus in F₂-hybrid males. Boxplot hinges are 25th and 75th quartiles, whiskers are 1.5× interquartile range, line at median. *P*-value by ANOVA.

Logarithm of the odds (LOD) across the genome of **d**, *Hif1a* and **e**, *Runx2* expression. **f**, LOD across the genome for the TF module and the TF module excluding *Gadd45a*. **g**, LOD of the TF module and the TF module controlling for *Gadd45a* expression. Dashed lines denote genome-wide threshold of significance ($\alpha = 0.05$).



Extended Data Fig. 10 | Cis-regulation of *Tnn* contributes to extracellular matrix module expression. **a**, Expression of *Tnn* in deer and oldfield mice.

P-value by two-sided *t*-test. **b**, Allele-specific expression of *Tnn* in deer × oldfield F₁ hybrids. *P*-value by paired two-sided *t*-test. **c**, Correlation between *Akr1c18* expression and *Tnn* expression across development of oldfield mice. *P*-value by bivariate correlation, *R* denotes Pearson's correlation coefficient. **d**, Logarithm of the odds (LOD) across the genome of *Cdkn2a*, *Podnl1*, *Serpine1*, and *Timp1* expression. **e**, LOD of the ECM module and the ECM module without *Tnn*. **f**, LOD

of the ECM module and the ECM module controlling for *Tnn* expression. **g**, LOD of *Akr1c18* expression and *Akr1c18* expression controlling for *Tnn* expression. Dashed lines denote genome-wide threshold of significance ($\alpha = 0.05$). **h**, *Tnn* expression as a function of genotype at the *Tnn* locus in F₂-hybrid males. *Akr1c18* expression as a function of genotype at the *Tnn* locus (**i**) or the *Akr1c18* locus (**j**) in F₂-hybrid males. **h,j** Boxplot hinges are 25th and 75th quartiles, whiskers are 1.5× interquartile range, line at median. *P*-values by ANOVA.

Reporting Summary

Nature Portfolio wishes to improve the reproducibility of the work that we publish. This form provides structure for consistency and transparency in reporting. For further information on Nature Portfolio policies, see our [Editorial Policies](#) and the [Editorial Policy Checklist](#).

Please do not complete any field with "not applicable" or n/a. Refer to the help text for what text to use if an item is not relevant to your study. [For final submission:](#) please carefully check your responses for accuracy; you will not be able to make changes later.

Statistics

For all statistical analyses, confirm that the following items are present in the figure legend, table legend, main text, or Methods section.

n/a Confirmed

- The exact sample size (n) for each experimental group/condition, given as a discrete number and unit of measurement
- A statement on whether measurements were taken from distinct samples or whether the same sample was measured repeatedly
- The statistical test(s) used AND whether they are one- or two-sided
Only common tests should be described solely by name; describe more complex techniques in the Methods section.
- A description of all covariates tested
- A description of any assumptions or corrections, such as tests of normality and adjustment for multiple comparisons
- A full description of the statistical parameters including central tendency (e.g. means) or other basic estimates (e.g. regression coefficient) AND variation (e.g. standard deviation) or associated estimates of uncertainty (e.g. confidence intervals)
- For null hypothesis testing, the test statistic (e.g. F , t , r) with confidence intervals, effect sizes, degrees of freedom and P value noted
Give P values as exact values whenever suitable.
- For Bayesian analysis, information on the choice of priors and Markov chain Monte Carlo settings
- For hierarchical and complex designs, identification of the appropriate level for tests and full reporting of outcomes
- Estimates of effect sizes (e.g. Cohen's d , Pearson's r), indicating how they were calculated

Our web collection on [statistics for biologists](#) contains articles on many of the points above.

Software and code

Policy information about [availability of computer code](#)

Data collection Nikon Elements and NeuroLucida were used to obtain microscopy images.

Data analysis Bulk and single-cell RNA-sequencing data was analyzed using the following software as described in the methods: Trimmomatic v0.36, STAR aligner v2.6.0a, RSEM v1.3.3, DESeq2 v1.36.0, kallisto v0.46.0, mmseq v1.0.11, 10X Genomics CellRanger v7.1, pheatmap v1.0.12, CellBender v0.3.0, and Seurat v4.3.0. Data was plotted in R version 4.2.1 using ggplot2 v3.4.0. ImageJ was used to analyze adrenal volume. Electrophysiology data were analyzed using AxographX and IgorPro (Wavemetrics). Expression QTL mapping was performed using R/qtL.

For manuscripts utilizing custom algorithms or software that are central to the research but not yet described in published literature, software must be made available to editors and reviewers. We strongly encourage code deposition in a community repository (e.g. GitHub). See the Nature Portfolio [guidelines for submitting code & software](#) for further information.

Data

Policy information about [availability of data](#)

All manuscripts must include a [data availability statement](#). This statement should provide the following information, where applicable:

- Accession codes, unique identifiers, or web links for publicly available datasets
- A description of any restrictions on data availability
- For clinical datasets or third party data, please ensure that the statement adheres to our [policy](#)

Sequencing data can be found at BioProject ID PRJNA1094591. All other source data can be found in Supporting Information.

Research involving human participants, their data, or biological material

Policy information about studies with [human participants or human data](#). See also policy information about [sex, gender \(identity/presentation\), and sexual orientation](#) and [race, ethnicity and racism](#).

Reporting on sex and gender

N/A

Reporting on race, ethnicity, or other socially relevant groupings

N/A

Population characteristics

N/A

Recruitment

N/A

Ethics oversight

N/A

Note that full information on the approval of the study protocol must also be provided in the manuscript.

Field-specific reporting

Please select the one below that is the best fit for your research. If you are not sure, read the appropriate sections before making your selection.

Life sciences Behavioural & social sciences Ecological, evolutionary & environmental sciences

For a reference copy of the document with all sections, see nature.com/documents/nr-reporting-summary-flat.pdf

Life sciences study design

All studies must disclose on these points even when the disclosure is negative.

Sample size

For some experiments, sample sizes were calculated based on power analyses. In others, sample sizes were not predetermined and instead conform or are well above the standard in the field (see Button, K., Ioannidis, J., Mokrysz, C. et al. Power failure: why small sample size undermines the reliability of neuroscience. *Nat Rev Neurosci* 14, 365–376 (2013). <https://doi.org/10.1038/nrn3475>).

Data exclusions

Data were not excluded from analysis.

Replication

In behavioral experiments, independent investigators scored (blindly) the same videos, arriving at nearly identical results. Antibody staining and *in situ* hybridization experiments were performed multiple times on independent samples.

Randomization

Animals for experiments were taken at random (given appropriate age and sex) from our laboratory colonies for experiments and assigned to treatment balanced with respect to litter of origin, sex, and age.

Blinding

Investigators were blind to treatment when scoring behavior videos. Experimenter blinding to species was not relevant or feasible, given the enormous differences between groups but experimenters were blind to the treatment of the animals.

Reporting for specific materials, systems and methods

We require information from authors about some types of materials, experimental systems and methods used in many studies. Here, indicate whether each material, system or method listed is relevant to your study. If you are not sure if a list item applies to your research, read the appropriate section before selecting a response.

Materials & experimental systems

- | | |
|-------------------------------------|-----------------------------------------------------------------|
| n/a | Involved in the study |
| <input type="checkbox"/> | <input checked="" type="checkbox"/> Antibodies |
| <input checked="" type="checkbox"/> | <input type="checkbox"/> Eukaryotic cell lines |
| <input checked="" type="checkbox"/> | <input type="checkbox"/> Palaeontology and archaeology |
| <input type="checkbox"/> | <input checked="" type="checkbox"/> Animals and other organisms |
| <input checked="" type="checkbox"/> | <input type="checkbox"/> Clinical data |
| <input checked="" type="checkbox"/> | <input type="checkbox"/> Dual use research of concern |
| <input checked="" type="checkbox"/> | <input type="checkbox"/> Plants |

Methods

- | | |
|-------------------------------------|-------------------------------------------------|
| n/a | Involved in the study |
| <input checked="" type="checkbox"/> | <input type="checkbox"/> ChIP-seq |
| <input checked="" type="checkbox"/> | <input type="checkbox"/> Flow cytometry |
| <input checked="" type="checkbox"/> | <input type="checkbox"/> MRI-based neuroimaging |

Antibodies

Antibodies used	Anti-Rbfox1 (EMD Millipore, MABE159, lot #2584875) used at 1:1000 Anti-tyrosine hydroxylase (EMD Millipore AB152, lot #3236358) used at 1:1000 Donkey anti-rabbit Alexa Fluor 647, Invitrogen A-31573, Lot #1874788, 1:1000
Validation	The anti-Rbfox1 antibody has been validated for western blotting by the manufacturer. Anti-Rbfox1 was validated for use on Peromyscus tissue using antibody titration experiments. The anti-tyrosine hydroxylase antibody has been published and validated for use in ELISA, IF, IH, IH(P), IP and WB by the manufacturer. This antibody reacts with a variety of species including mice, rats, humans, flies, and mollusks. The secondary antibody has been validated by the manufacturer in western blots.

Animals and other research organisms

Policy information about [studies involving animals](#); [ARRIVE guidelines](#) recommended for reporting animal research, and [Sex and Gender in Research](#)

Laboratory animals	Deer mice (<i>Peromyscus maniculatus bairdii</i> , strain BW), oldfield mice (<i>Peromyscus polionotus subgriseus</i> , strain PO), California mice (<i>Peromyscus californicus</i>), white-footed mice (<i>Peromyscus leucopus</i>), the Santa Rosa Island beach mouse (<i>Peromyscus polionotus leucocephalus</i>), and the cloudland deer mouse (<i>Peromyscus maniculatus nubiterrae</i>) were used for experiments including adrenal harvest (ages P0-P500), blood draw (P55-P85) and parental behavior experiments (P60-P120). C57BL/6J mice were used for adrenal scRNASeq experiments. Adrenal histology was performed on adults (P60-P120) except where stated.
Wild animals	No wild animals were used in this study.
Reporting on sex	Both sexes were used in these experiments.
Field-collected samples	No field-collected samples were used in this study.
Ethics oversight	The <i>Peromyscus</i> work was performed under the study protocol AC-AAAT0450 and AC-AABH6555 as approved by the Institutional Animal Care and Use Committee of Columbia University and Albert Einstein College of Medicine.

Note that full information on the approval of the study protocol must also be provided in the manuscript.

Plants

Seed stocks	N/A
Novel plant genotypes	N/A
Authentication	N/A

